Available online at www.sciencedirect.com
ScienceDirect
Journal of Computational Physics 220 (2006) 312–338
JOURNAL OF COMPUTATIONAL PHYSICS
www.elsevier.com/locate/jcp

A well-balanced approach for flows over mobile-bed with high sediment-transport

G. Rosatti *, L. Fraccarollo

Centro Universitario per la Difesa idrogeologica dell'Ambiente Montano (CUDAM), Dipartimento Ingegneria Civile e Ambientale, Università degli Studi di Trento, Via Mesiano, 77 I-38050 Trento, Italy

Received 8 November 2005; received in revised form 31 March 2006; accepted 12 May 2006
Available online 30 June 2006

Abstract

In this paper we deal with the numerical computation of one-dimensional, unsteady, free-surface flows over mobile-bed. We focus on flows characterized by high concentration of sediments and strong interaction between flow and bottom dynamics, as in hyper-concentrated- and debris-flows. These features are fully considered in the adopted system of equations. Challenging in its numerical approximation is the preservation of the coupling and the treatment of a non-conservative flux in the momentum equation. In order to devise a new Godunov-type approach, we analyzed in detail the Riemann problem associated with the mobile-bed phenomena and the peculiar features of its wave relations. The scheme we developed is based on two supports: well-balanced treatment of the variable updating at the new time-level and flux evaluation by three-wave approximations of the intercell Riemann-problem that, without any split, embody the effect of the non-conservative term. The properties of the new numerical strategy (named AWB) are assessed by comparison with exact solutions of Riemann problems, built by handling an inverse technique. Finally, AWB has been applied to cases of practical interest, where wave interaction and friction effects makes the flow more complex. The obtained results point out that the new method is able to predict faithfully the overall behaviour of the solution and of any type of waves. The use of AWB, in this one-dimensional frame, is therefore fostered in representing rapid transients in river/torrent flows with movable bed.

Keywords: Well-balanced scheme; Riemann solvers; Non-conservative term; Mobile-bed models; Sediment transport

1. Introduction

The object of the work is to devise a numerical approach able to deal with a class of phenomena quite important in mountain areas, that is the propagation of floods inside gullies, torrent or rivers after heavy rain, or induced by the abrupt collapse of natural/artificial barriers. A crucial feature of the flows we consider is that they transport sediments and induce morphological variations, that is erosional and depositional processes. In these conditions the sediments may transfer from rest, in the bed, to motion and vice versa. This refers to

* Corresponding author. Tel.: +39 0461882621; fax: +39 0461882672.
E-mail addresses: giorgio.rosatti@ing.unitn.it (G. Rosatti), luigi.fraccarollo@ing.unitn.it (L. Fraccarollo).

0021-9991/$ - see front matter
doi:10.1016/j.jcp.2006.05.012

sediment-laden flows over mobile-bed, as reported in the title. We restrict the attention to problems with a fluid-like general behaviour, and exclude therefore landslide, dry-mass movements and problems with heavy geotechnical implications, such as breach- and bank-ruptures. The main elements laying at the core of our mathematical approach consist of immediate-equilibrium hypothesis and full coupling. Immediate-equilibrium means that the solid discharge is linked to the local flow conditions via an algebraic relation, representing the transport-capacity under uniform conditions. This choice, although controversial in the state-of-the-art [7], may be substantiated on both theoretical and physical ground [13]. Actually, counter-measure works for debris flows, such as check dams and sieving systems, in Alps and in Japanese mountains, exploit the fast fitting of sediment concentration to flow velocity and viceversa, allowing deposition and stopping of the debris. Full coupling means that the mass and momentum exchanges through the bottom-interface Γ_b (Fig. 1) are considered in their effects on the bulk fluid-density and bed-level position. This issue, always neglected in ordinary sediment-transport problems, has to be considered in rapidly transient flows with high sediment transport.

As far as the numerics is concerned, the nature of the problems, which admit discontinuities, addressed us to exploit the capability of Godunov-type, finite-volume methods. The key point of these approaches consists of the solution of local Riemann problems at the cell-interfaces. A preliminary analysis of the mathematical model is therefore necessary in order to understand the possible wave-structures and the relations valid across shock and rarefaction waves as well. The partial differential equation (PDE) system, formed by three equations, is strictly hyperbolic (see Section 2). Peculiarity of it, as in all depth-averaged models (shallow water) is the presence of a non-conservative term in the momentum equation, expressing the pressure-thrust exerted on the bottom. This physical quantity gives also rise, in shock conditions, to relations with one more term than the standard Rankine–Hugoniot conditions for conservative problems (see Eq. 10). The expression of this term has to be obtained from the integral formulation of the problem and not from its differential one.

The coupling between bed and flow dynamics, and the non-conservative nature of the mobile-bed model, prevent a straightforward application of existing approaches without running into dramatic approximations or substantially wrong results, as it will be shown. In particular, our experience suggests that the treatment of the non-conservative term as a source term and the use of approximate Riemann solvers based on a reduced number of wave-fields, although widely applied in other problems, are to be avoided in the problem here considered. To the best of our knowledge, the only numerical-approach appeared in the literature that is applicable to the fully-coupled model faced in this paper is the LHLL method proposed in [14], a Godunov-type method based on the HLL Riemann-solver. The main innovation in LHLL is in the treatment of the non-conservative flux, which is managed in partially unsplitted way. It has been successfully applied to the benchmark case of the erosional dam-break flood over an initial horizontal-bed, first faced in [8]. Nevertheless, the application of this approach to some test-cases points out severe limitations in dealing with strong bed-variations. We found that the bed-steps are soon smeared out at a rate which is ruled out by the numerics and not by physical agents, leading, at some time, to a complete and wrong flattening of the bottom topography. In application to real cases these shortcomings enhance, and some new ways to obtaining satisfying numerical solutions have to be looked for. Unfortunately, the mentioned drawbacks are expected to affect

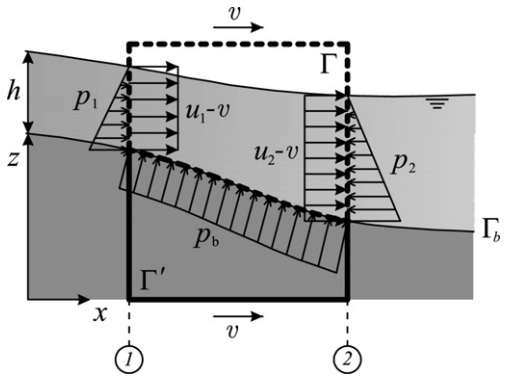

Fig. 1. Control volumes for the determination of the geomorphic shallow water equations.

all Godunov-type methods, including higher-order versions (e.g. ENO/WENO [11,17], ADER [27] and MUSTA [29] approaches), if they simplify the wave structure of the Riemann problem and consider the non-conservative flux splitted from the conservative ones. Classical central methods such as Lax–Friedrichs or Lax–Wrendroff (among the others) are expected to yield the very same limitations, as well. In this concern, grid refinement could also be helpful, but are not often feasible in real-cases, in which the choice of cell dimension is somehow constrained (often, in riverine computation, only a limited number of cross-sections are available).

In this paper we propose a new method, termed approximated well balanced (AWB), that is able to overcome the limits above-mentioned. Somehow, it can be considered as a generalization to the mobile bed-case of the original well-balanced scheme by [16,10], devoted to shallow-water flows of clear water. The core of the approach dwells in the solution of the intercell Riemann-problem, which has to take into account the non-conservative term. This means to reach a solution with no splitting between conservative and non-conservative parts of the fluxes. To fully cope with well-balanced-scheme demands, the intercell fluxes have to come out from the exact solution of the Riemann problem, as in [10,16]. Unfortunately, for the problems considered in the present paper no exact solutions can be handled, at least in an efficient numerical-algorithm. Therefore, we propose Riemann-solvers that, although approximated, embody without any split the non-conservative term and, unlike HLL, consider the correct number of wave-fields. Our technique to achieve an approximate Riemann solution is presented in a general form and is applicable to other nonlinear hyperbolic set of PDE's, with expected improvements with respect to HLL applications. The well-balanced character of the scheme preserves the numerical solutions free from spurious effects in significant situations, such as the case of fluid at a steady rest ($\mathscr{C}$-property, [6]). In the end the new method shows the skill to deal with high slope-values and even with bed-steps under strong transient-stages of the flow. The method is presented in the first-order version because the main numerical-properties come out very clearly. Higher-order ones can be obtained from it quite straightforwardly.

In order to assess the quality of the numerical predictions, exact reference solutions have been obtained by solving an inverse problem, in the way outlined by [3,13]. Many exact solutions may therefore be considered. In the paper two of them have been selected, giving enough information relevant to the skill of any method to reproduce them. Finally, we have chosen a case of practical interest in the field of engineering river control, concerning the evolution of a trench initially dug in a river bed to extract, for the many possible purposes, sediments. In this application wave interactions and friction effects make the flow more complex, and no relevant exact solution is available; therefore we could just compare the results of AWB with the existing LHLL method.

The paper is structured as follows. At first the mathematical description of the problem is given (Section 2). In Section 3, the LHLL method is briefly described. The AWB scheme is then presented (Section 4); two new Riemann solvers are developed, based on a three-rarefaction or on three-shock approximation that, without any split, embody the effect of the non-conservative term (Section 5). Results are obtained from both AWB and LHLL for two tests with exact solution, and then for the evolving morphology associated to a trench dug in the bed (Section 6). Concluding remarks (Section 7) end the paper.

2. Mathematical description

The mathematical model used in this paper is similar to that described in [13]: we refer to this work for a detailed physical and theoretical framework. Moreover, we assume, as in [4], that the solid phase has a velocity equal to the liquid one and that it is uniformly distributed over the flow depth. Hereafter we present the mathematical aspects that are essential for the development of the numerical approach.

Integral form of the mathematical model can be derived from writing conservation laws referring to appropriate control-volumes. In order to obtain a formulation that allows to get the expression of the shock relations (Section 2.2) that are valid in this context, mobile control-volumes, moving in the x direction at a non-material speed v, must be employed.

$$\frac{\partial}{\partial t}\int_{x_1}^{x_2}(h+z)\,\mathrm{d}x + [(u-v)h - zv]_{x_1}^{x_2} = 0, \tag{1a}$$

$$\frac{\partial}{\partial t}\int_{x_1}^{x_2}(ch+c_\mathrm{b}z)\,\mathrm{d}x + [ch(u-v) - c_\mathrm{b}zv]_{x_1}^{x_2} = 0, \tag{1b}$$

$$\frac{\partial}{\partial t}\int_{x_1}^{x_2}(uh(c\Delta+1))\,\mathrm{d}x+\left[(c\Delta+1)\left(uh(u-v)+g\frac{h^2}{2}\right)\right]_{x_1}^{x_2}-\int_{x_1}^{x_2}\frac{p_{bx}}{\rho_w}\,\mathrm{d}\Gamma_b=-\int_{x_1}^{x_2}\frac{\tau}{\rho_w}\,\mathrm{d}\Gamma_b. \tag{1c}$$

The first two equations of the system are obtained from the conservation of the mixture mass and the solid-phase mass, referring to the control volume $\Gamma+\Gamma'$ (see Fig. 1). The last equation derives from the momentum balance of the mixture, using Γ only. Variables are the mixture depth h, the depth-averaged velocity u and the elevation of the position of the bottom z; uh is the mixture flux, cuh is the sediment flux, where c is the volume concentration of sediments in the flow, c_b is the concentration of sediments in the bed ($c_b > c$), ρ_s is the density of the solid phase, ρ_w is the density of the water and $\Delta=(\rho_s-\rho_w)/\rho_w$ is the submerged relative density of the sediments. Γ and Γ' share the interface Γ_b, representing the bed-line, moving vertically with speed $\partial z/\partial t$.

Three further equations are needed to close the problem. The first one concerns the bed shear-stress τ. A general expression for it is:

$$\tau=\rho_w f u^2, \tag{2}$$

where f is a function of sediment shape, diameter and concentration. Well-known Chézy and Bagnold [26] relations are applicable to riverine and debris flows, respectively.

The second one must provide a relation between the concentration c and the primitive variables. For bed-load transport in rivers and torrents, an equilibrium approximation can be expressed by the following algebraic expression:

$$c=c_b\beta\frac{u^2}{h}, \tag{3}$$

where β is an empirical parameter [25]. The previous relation can be obtained by employing some classical expression for the transport capacity q_s, e.g., Ashida and Michiue [5] or Meyer-Peter and Müller [21]; this last one may be written as:

$$q_s=\frac{8}{g\Delta}\left(\frac{\tau}{\rho}-\frac{\tau_c}{\rho}\right)^{3/2}, \tag{4}$$

where g is gravity, Δ is the submerged relative density of the sediments, ρ is the fluid density and τ_c is a constant for a given grain-size. In problems with high sediment transport, as in the case we consider in the paper, $\tau_c \ll \tau$, and may be neglected. Now, by using Eq. (2), and being $q_s = cuh$, we finally obtain the expression (3).

The third one is necessary to express the integral x-component of the pressure along the bottom line Γ_b. The actual value of this term depends on the shape of the bed profile and on the pressure field; as a consequence, it cannot be expressed in a quite general form. Further in the paper we will provide some reasonable hypotheses under which it may be expressed in closed form. Importantly enough, the pressure thrust yields a term in the momentum equation that has to be considered as a non-conservative flux, and plays a role in Rankine–Hugoniot relations and in characteristic equations, as it will be exploited in the following sections.

As far as the subsequent mathematical description is concerned, the notation reported in Appendix A.1 is employed.

2.1. Standard integral formulation

Setting $v=0$, i.e. considering fixed control volumes, system (1) can be written in a more classical form:

$$\frac{\partial}{\partial t}\int_{x_1}^{x_2}\mathbf{U}\,\mathrm{d}x+\mathbf{F}|_{x_2}-\mathbf{F}|_{x1}-\int_{x_1}^{x_2}\mathbf{P}\,\mathrm{d}\Gamma_b=\int_{x_1}^{x_2}\mathbf{S}\,\mathrm{d}\Gamma_b, \tag{5}$$

where

$$\mathbf{U}=\begin{pmatrix}h+z\\ ch+c_b z\\ uh(c\Delta+1)\end{pmatrix},\quad \mathbf{F}=\begin{pmatrix}uh\\ cuh\\ (c\Delta+1)\left(u^2h+g\frac{h^2}{2}\right)\end{pmatrix},\quad \mathbf{P}=\begin{pmatrix}0\\ 0\\ \frac{p_{bx}}{\rho_w}\end{pmatrix},\quad \mathbf{S}=\begin{pmatrix}0\\ 0\\ -\frac{\tau}{\rho_w}\end{pmatrix}. \tag{6}$$

This formulation will be used further in the paper (Section 4) to obtain a well-balanced approach. The bottom-stress term (in **S**) is a classical source term, and will not be considered in the following development. This choice does not means that the fluid is considered inviscid, since the effect of the shear stress is fully considered in causing the sediment movement (see derivation of Eq. (3)). Without this source term, anyway, the model remains realistic in representing the first stages of flows in Riemann problems, as shown for the dam-break case in [13]. The bottom shear-stress in **S** will be reconsidered dealing with cases of practical interest, later proposed, where it plays a significant role.

2.2. Shock relations

The equations valid across a shock discontinuity propagating at a constant speed $S^{i-1,i}$ between constant states $i-1$ and i can be derived from system (1), by setting the control-volume velocity v equal to the shock speed $S^{i-1,i}$ (Fig. 2). Being the flow stationary in the moving reference-system, temporal terms drop out, and the first two conservation laws (Eqs. (1a) and (1b)) provide the following relations:

$$F_j^i - F_j^{i-1} = S^{i-1,i}\left(U_j^i - U_j^{i-1}\right), \quad j = 1,2 \tag{7}$$

which are the standard Rankine–Hugoniot relations (hereafter, RH). The third equation (Eq. (1c)) comprises the x-component of pressure along the bottom which, in this case, becomes a thrust over a vertical step ($D_3^{i-1,i}$ in Fig. 2). Its evaluation would actually require to know the two-dimensional flow around the bottom step, which is another scientific topic. In a one-dimensional frame this closure-problem may be faced by reasonable assumptions. In the following we assume that the pressure distribution in the mixture is hydrostatic over the vertical step, and that the pressure head depends only on the free-surface level in either side of the discontinuity where the bottom elevation is lower.

With reference to Fig. 2, we finally consider:

$$D_3^{i-1,i} = g(c_j \Delta + 1)\left(h_j - \frac{|\zeta^{i-1,i}|}{2}\right)\zeta^{i-1,i}, \tag{8}$$

where $\zeta^{i-1,i} = z^{i-1} - z^i$, and

$$j = \begin{cases} i-1 & \text{if } z^{i-1} \leqslant z^i, \\ i & \text{if } z^{i-1} > z^i. \end{cases}$$

Nevertheless, different expressions from (8) could be considered as well, without changes in the theoretical and numerical approach outlined in subsequent paragraphs. Eq. (1c) reads now:

$$F_3^i - F_3^{i-1} - D_3^{i-1,i} = S^{i-1,i}\left(U_3^i - U_3^{i-1}\right) \tag{9}$$

which represents the RH relation for the momentum equation.

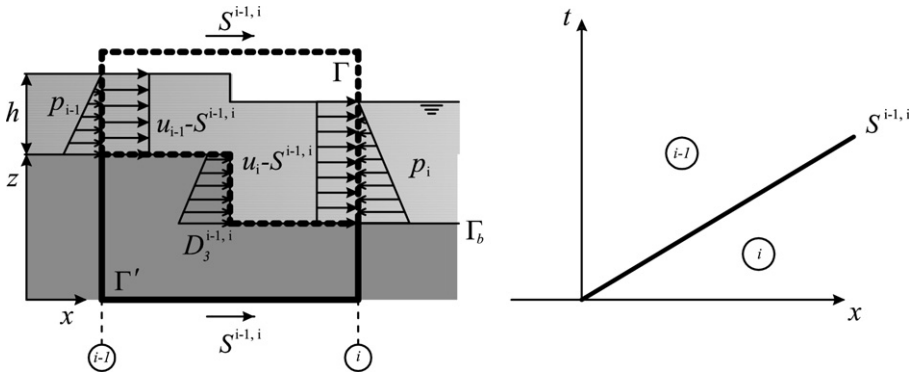

Fig. 2. Control volumes used to obtain Rankine–Hugoniot type shock-relation.

In compact form the RHs become:

$$\mathbf{F}^i - \mathbf{F}^{i-1} - \mathbf{D}^{i-1,i} = S^{i-1,i}(\mathbf{U}^i - \mathbf{U}^{i-1}), \tag{10}$$

where $\mathbf{D}^{i-1,i} = [0, 0, D_3^{i-1,i}]^{\mathrm{T}}$ is the vector of thrust terms.

A final remark concerns the entropy relation which must be satisfied by the shock in order to be physically acceptable:

$$\lambda_i^{i-1} > S^{i-1,i} > \lambda_i^i \tag{11}$$

being λ_i^{i-1} and λ_i^i the ith eigenvalues, upstream and downstream of the shock, respectively.

2.3. Eigenstructure and the linearized characteristic equations

Assuming smooth variation of the variables and almost parallel profiles of the free surface and of the bed, the pressure is hydrostatic through the flow depth, and it therefore comes out:

$$\frac{p_{\mathrm{b}x}}{\rho_{\mathrm{w}}} = -gh(c\Delta + 1)\frac{\partial z}{\partial x}. \tag{12}$$

It is worthwhile observing that the integral expression (8) is consistent with the above differential one when the step is infinitesimal. On the contrary, integration of Eq. (12) cannot be worked out to recover expression (8) when the bottom is discontinuous. The PDEs system can be then obtained from (5) as result of the limit $x_2 \to x_1$, and in compact form it is:

$$\frac{\partial \mathbf{U}}{\partial t} + \frac{\partial \mathbf{F}}{\partial x} + \mathbf{H}\frac{\partial z}{\partial x} = 0, \tag{13}$$

where

$$\mathbf{H} = \begin{pmatrix} 0 \\ 0 \\ gh(c\Delta + 1). \end{pmatrix}. \tag{14}$$

Eq. (13) can be written in quasi-linear form using the closure relation (3) for the concentration:

$$\mathbf{B}(\mathbf{W})\frac{\partial \mathbf{W}}{\partial t} + \mathbf{A}(\mathbf{W})\frac{\partial \mathbf{W}}{\partial x} = 0, \tag{15}$$

where

$$\mathbf{W} = \begin{bmatrix} h \\ u \\ z \end{bmatrix}, \quad \mathbf{B} = \begin{pmatrix} 1 & 0 & 1 \\ 0 & 2\beta c_{\mathrm{b}} u & c_{\mathrm{b}} \\ u & 3qu^2 + h & 0 \end{pmatrix}, \tag{16}$$

$$\mathbf{A} = \begin{pmatrix} u & h & 0 \\ 0 & 3\beta c_{\mathrm{b}} u^2 & 0 \\ \frac{1}{2}ru^2 + gh & (4qu^2 + rh)u & k \end{pmatrix} \tag{17}$$

and $k = gh(c\Delta + 1)$, $q = \beta c_{\mathrm{b}}\Delta$, $r = qg + 2$.

The eigenvalues of system (15) are calculated from the relationship:

$$\det(\mathbf{A} - \lambda\mathbf{B}) = 0, \tag{18}$$

which results to be the third-order polynomial reported in Appendix A.2. The three solutions, as shown in [22] or [13], are real and distinct, and therefore the geomorphic problem is strictly hyperbolic. Two eigenvalues have the same sign of particle velocity u, one is opposite. We name them in ascending order: with $u > 0$, it is $\lambda_1 < 0$, $\lambda_2 \geqslant 0$, $\lambda_3 > 0$ and $\lambda_3 > \lambda_2$, while $\lambda_2 = 0$ only if $u = 0$, i.e. the condition of fluid at rest.

The right eigenvector associated to λ_i, written in term of primitive variables, is

$$\mathbf{K}_i = \begin{pmatrix} -\lambda_i(-u\beta(3u-2\lambda_i)+h) \\ \lambda_i(u-\lambda_i) \\ (u\beta(3u-2\lambda_i))(u-\lambda_i) \end{pmatrix}. \tag{19}$$

It is easy to verify that for the condition of water at rest $\mathbf{K}_2 = 0$ and also $\nabla\lambda_2 \cdot \mathbf{K}_2 = 0$; therefore the λ_2-field is not genuinely nonlinear while the other fields are genuinely nonlinear.

A linearized expression of the characteristic equations associated to system (15), that will be used further in the paper (Section 5.2), is the following:

$$\mathbf{C}\left(\frac{\partial \mathbf{W}}{\partial t} + \mathbf{\Lambda}\frac{\partial \mathbf{W}}{\partial x}\right) = 0, \tag{20}$$

where

$$\mathbf{\Lambda} = \begin{bmatrix} \lambda_1 & 0 & 0 \\ 0 & \lambda_2 & 0 \\ 0 & 0 & \lambda_3 \end{bmatrix}, \quad \mathbf{C} = \begin{bmatrix} \mathbf{C}_1 \\ \mathbf{C}_2 \\ \mathbf{C}_3 \end{bmatrix} = \mathbf{TB}, \quad \mathbf{T} = \begin{bmatrix} \mathbf{T}_1 \\ \mathbf{T}_2 \\ \mathbf{T}_3 \end{bmatrix} \tag{21}$$

and $\mathbf{T}_i$, the left ith eigenvector associated to the ith eigenvalue, is

$$\mathbf{T}_i = \begin{pmatrix} -\lambda_i(s-\lambda_i u) & \frac{\lambda_i}{c_b}(s-\lambda_i u) + \frac{(u-\lambda_i)}{c_b}k & (u-\lambda_i)\lambda_i \end{pmatrix} \tag{22}$$

being $s = \frac{1}{2}ru^2 + gh$. The expression of $\mathbf{C}_i$ as function of $\mathbf{W}$ and λ_i is reported in Appendix A.3.

In explicit form, Eq. (20) writes:

$$C_{i,1}\,\mathrm{d}h + C_{i,2}\,\mathrm{d}u + C_{i,3}\,\mathrm{d}z = 0, \text{ along } \frac{\mathrm{d}x}{\mathrm{d}t} = \lambda_i, \quad \text{with } i = 1,3. \tag{23}$$

Integrating along the ith characteristic, and assigning $C_{i,j}$ an average value $\overline{C}_{i,j} = C_i(\hat{\mathbf{W}}, \hat{\lambda}_i)$, where $\hat{\mathbf{W}}, \hat{\lambda}_i$ are suitable values of the primitive variables and of the eigenvalues, the following linearized characteristic-equations are obtained:

$$\overline{\mathbf{C}}_i \cdot \Delta\mathbf{W} = 0, \quad \text{with } i = 1,3, \tag{24}$$

where $\Delta\mathbf{W} = [\Delta h,\ \Delta u,\ \Delta z]^{\mathrm{T}}$ is the vector of the variations of the primitive variables along each characteristic-line. $\overline{\mathbf{C}}_i$ can be considered a vector of weights ruling out the primitive-variable changes along the ith characteristic.

3. The LHLL approach

In Sections 3 and 4 we deal with numerics, and the standard numerical notation is employed, where the subscripts refer to the grid-position, and superscripts to time level. To the best of our knowledge, the only numerical approach appeared in the literature, that can be applied straightforwardly to system (13), is that one proposed in [14]. This method, called LHLL, has been used to integrate a system of PDEs very similar to (13) and has been successfully applied to the erosional dam-break flood over an initial horizontal bed; the comparison between the numerical results and experimental data was satisfactory [14]. LHLL is a finite-volume Godunov-type one and is based on a HLL [18] scheme for the homogeneous conservative-part of the system, and on a discretization of the non-conservative term with a "lateralization" approach: this leads to a definition of two numerical fluxes for each interface, one for the right side, $\mathbf{F}^{+}_{i+1/2}$, and one for the left side, $\mathbf{F}^{-}_{i+1/2}$. For system (13), the resulting explicit expression for the flux is the following:

$$\mathbf{F}^{\pm}_{i+1/2} = \mathbf{F}^{\mathrm{HLL}} + \frac{S^{\pm}}{S^{+} - S^{-}}\tilde{\mathbf{H}}\left(z^n_{i+1} - z^n_i\right), \tag{25}$$

where $\tilde{\mathbf{H}} = 0.5(\mathbf{H}^n_i + \mathbf{H}^n_{i+1})$ and $S^{\pm}$ are the velocity of the fastest and the slowest waves of the RP, respectively. In order to respect the $\mathscr{C}$-property [6], and to avoid some unphysical results, solid mass numerical fluxes F_2 must be less than the total mass fluxes F_1, and this is achieved with the following limiter:

$$F_2 = \text{minmod}\,[F_2, F_1]. \tag{26}$$

We address to the original work [14] for a more detailed description and properties of the approach that leads to (25) and (26). In Section 5.1.3 an interpretation of this method, in the framework of our new approach, will be given. All considered, the lateralization technique copes with the non-conservative term in an unsplit way, and not as a source term (i.e, by splitting technique).

Despite its successful application to the erosional dam-break problem, in more general situations the LHLL method has shown some significant limits that prevent the use of this scheme in practical application. This fact induced the writers to search for better schemes.

4. A well-balanced scheme for the movable-bed equations

The numerical approach we are going to present belongs to the well-balanced (WB) family, a class of explicit schemes, introduced by [16,19] for rigid-bed flows, which can be considered an extension of the Godunov [15] numerical approach to hyperbolic systems with stiff source and/or non-conservative terms. WB schemes are completely unsplitted approaches since they consider these last terms both into the solution of Riemann problems and to update the conserved variables. In the following, we will present a first-order scheme, leaving extensions to higher orders to forthcoming work. We assume constant cell-size Δx, the center of which is located at position x_i, whereas the intercell positions around x_i are $x_{i-1/2} = x_i - \Delta x/2$ and $x_{i+1/2} = x_i + \Delta x/2$.

In general, finite-volume schemes are obtained integrating a system of PDEs over $(t^n, t^{n+1}) \times (x_{i-1/2}, x_{i+1/2})$. Nevertheless we have already stressed as the space integration of PDE system (13) leads to integral form (5) only if the solution is smooth. Therefore, in order to manage a general expression, Eq. (5), is evaluated between $x_2 = x_{i+1/2}$, $x_1 = x_{i-1/2}$ and integrated over (t^n, t^{n+1}):

$$\int_{t^n}^{t^{n+1}} \left(\frac{\partial}{\partial t} \int_{x_{i-1/2}}^{x_{i+1/2}} \mathbf{U}(x,t)\,\mathrm{d}x + \mathbf{F}(\mathbf{U}(x_{i+1/2},t)) - \mathbf{F}(\mathbf{U}(x_{i-1/2},t)) - \int_{x_{i-1/2}}^{x_{i+1/2}} \mathbf{P}(x,t)\,\mathrm{d}\Gamma_\mathrm{b} \right) \mathrm{d}t = 0. \tag{27}$$

With the following standard cell-average definitions,

$$\mathbf{U}_i^n = \frac{1}{\Delta x} \int_{x_{i-1/2}}^{x_{i+1/2}} \mathbf{U}(x,t^n)\,\mathrm{d}x, \tag{28}$$

$$\mathbf{F}_{i\pm1/2} = \frac{1}{\Delta t} \int_{t^n}^{t^{n+1}} \mathbf{F}(\mathbf{U}(x_{i\pm1/2},t))\,\mathrm{d}t, \tag{29}$$

$$\mathbf{P}_i = \frac{1}{\Delta t} \int_{t^n}^{t^{n+1}} \int_{x_{i-1/2}}^{x_{i+1/2}} \mathbf{P}(x,t)\,\mathrm{d}\Gamma_\mathrm{b}\,\mathrm{d}t, \tag{30}$$

the relevant compact expression becomes:

$$\mathbf{U}_i^{n+1} = \mathbf{U}_i^n - \frac{\Delta t}{\Delta x}(\mathbf{F}_{i+1/2} - \mathbf{F}_{i-1/2} - \mathbf{P}_i). \tag{31}$$

In the framework of a WB approach, the updated conserved variable $\mathbf{U}_i^{n+1}$ comes out from a cell-average after the evolution of the local RPs on either side of the cell (see e.g. [28, Chapter 6]). With an equivalent statement, numerical fluxes can be expressed as

$$\mathbf{F}_{i+1/2} = \mathbf{F}(\mathbf{U}_{i+1/2}^n(0)), \tag{32}$$

where $\mathbf{U}_{i+1/2}^n(x/t)$ is the self-similar solution of the local RP with left initial condition $\mathbf{U}_i^n$ and right initial one $\mathbf{U}_{i+1}^n$. Likewise, $\mathbf{F}_{i-1/2} = \mathbf{F}(\mathbf{U}_{i-1/2}^n(0))$. Also the value of $\mathbf{P}_i$ must come out from the same RP solution, but being $\mathbf{P}(x,t)$ not available in analytical form, it is not easy to be evaluated.

A direct procedure to obtain exact solutions of the RPs is not readily available. Therefore, we propose to use approximate Riemmann-solvers that are able to keep the main features of the exact solution, i.e. wave-structure and unsplit evaluation of the pressure term. In Section 5 some solvers with this property will be provided. We also propose an approximate expression for $\mathbf{P}_i$ assuming a step-wise configuration of each wave-field. In this way the pressure term is approximated as a sum of thrusts, each one calculated by

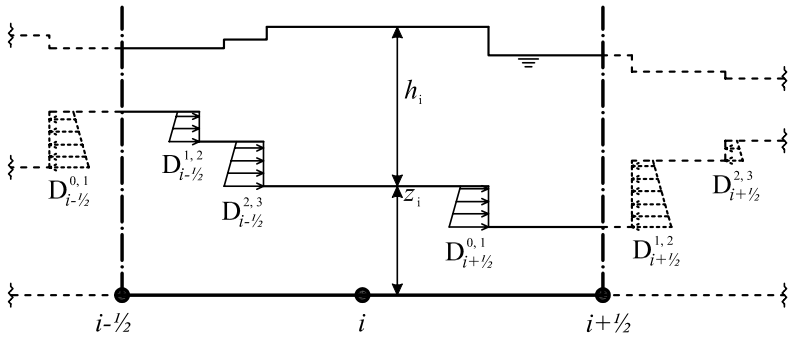

Fig. 3. Schematic of the AWB approximation of the flow-field evolution in the ith cell due to the two intercell RPs.

Eq. (8). Moreover, between two subsequent fields in the RP solution, the bed is horizontal and no pressure in x-direction is exerted over it. The spatial integral in (30) is therefore supplied only with contributions $\mathbf{D}^{m-1,m}$ coming from the wave-fields affecting the cell (see Fig. 3). At last, because of the self-similar character of the RP solution, any $\mathbf{D}^{m-1,m}$ is time independent and then $\mathbf{P}_i$ becomes:

$$\mathbf{P}_i \simeq \sum_{m=k_{i-1/2}}^{3} \mathbf{D}_{i-1/2}^{m-1,m} + \sum_{m=1}^{k_{i+1/2}} \mathbf{D}_{i+1/2}^{m-1,m}, \tag{33}$$

where $k_{i\pm1/2}$ are, respectively, the first and the last ordered number of waves that lay inside the cell. Their values depends on the sign of the velocities of the developing RPs: in case of positive particle-velocity all over the solution, as in Fig. 3, waves inside the cell are the first field of the downstream RP (i.e., $k_{i+1/2} = 1$), and the second and third fields of the upstream RP (i.e. $k_{i-1/2} = 2$). In this case we obtain:

$$\mathbf{P}_i \simeq \mathbf{D}_{i+1/2}^{0,1} + \mathbf{D}_{i-1/2}^{1,2} + \mathbf{D}_{i-1/2}^{2,3}. \tag{34}$$

We are able to provide the final expression of the proposed approximated well-balanced (AWB) scheme:

$$\mathbf{U}_i^{n+1} = \mathbf{U}_i^n - \frac{\Delta t}{\Delta x}(\mathbf{F}_{i+1/2}^- - \mathbf{F}_{i-1/2}^+), \tag{35}$$

where

$$\mathbf{F}_{i-1/2}^+ = \mathbf{F}_{i-1/2} + \sum_{m=k_{i-1/2}}^{3} \mathbf{D}_{i-1/2}^{m-1,m}, \quad \mathbf{F}_{i+1/2}^- = \mathbf{F}_{i+1/2} + \sum_{m=1}^{k_{i+1/2}} \mathbf{D}_{i+1/2}^{m-1,m} \tag{36}$$

and $\mathbf{F}_{i\pm1/2}$ are obtained by

$$\mathbf{F}_{i\pm1/2} = \mathbf{F}(\tilde{\mathbf{U}}_{i\pm1/2}^n(0)), \tag{37}$$

where $\tilde{\mathbf{U}}_{i+1/2}^n(0)$ is the approximated solution of the RPs. In order to ensure the stability of the numerical scheme, the well known following CFL condition must be verified:

$$\Delta t \leqslant \frac{\Delta x}{|\lambda_{\mathrm{M}}|},$$

where $|\lambda_{\mathrm{M}}|$ is the maximum wave speed of each local RP.

Several properties of the scheme above presented depend on the choice of the approximated solver used in (37). Anyhow, some general features can be highlighted.

The first issue concerns the skill of the methods to capture the shocks at the right strength (and speed, as a consequence). Following [20], let us consider a problem with initial value $\mathbf{u}_0(x)$ and constant boundary-conditions at $x = 0$ and $x = M\Delta x$ for the time-period $0 \leqslant t \leqslant N\Delta t$. Setting $\mathbf{U}_i^0$ equal to the ith cell-averaged initial value, it holds:

$$\int_0^{M\Delta x} \mathbf{u}_0(x)\,\mathrm{d}x = \Delta x \sum_{i=0}^{M} \mathbf{U}_i^0. \tag{38}$$

At time $t = N\Delta t$, the integral of the exact solution over the domain $[0, M\Delta x]$ can be written in the following form:

$$\int_0^{M\Delta x} \mathbf{u}(x, N\Delta t)\,\mathrm{d}x = \int_0^{M\Delta x} \mathbf{u}_0(x)\,\mathrm{d}x - N\Delta t[\mathbf{F}|_{x=M\Delta x} - \mathbf{F}|_{x=0}] - \int_0^{N\Delta t}\int_0^{M\Delta x} \mathbf{P}(x,t)\,\mathrm{d}\Gamma_\mathrm{b}\,\mathrm{d}t, \tag{39}$$

where $\mathbf{F}$ is the physical flux function.

Instead, the numerical approximation of the previous integral can be obtained from Eq. (31) by using both the telescopic and the consistency property of the numerical fluxes $\mathbf{F}_{i\pm1/2}$:

$$\Delta x \sum_{i=0}^{M} \mathbf{U}_i^N = \Delta x \sum_{i=0}^{M} \mathbf{U}_i^0 - N\Delta t \left[\mathbf{F}|_{x=M\Delta x} - \mathbf{F}|_{x=0} + \sum_{i=0}^{M}\left(\sum_{j=0}^{N} \mathbf{P}_i^j\right)\right]. \tag{40}$$

By comparing Eq. (40) with Eq. (39), it becomes clear that the space-integral of the numerical state-variable $\mathbf{U}$, over the whole flow domain at any time-level N, is exact only if:

$$\sum_{i=0}^{M}\left(\sum_{j=0}^{N} \mathbf{P}_i^j\right) = \int_0^{N\Delta t}\int_0^{M\Delta x} \mathbf{P}(x,t)\,\mathrm{d}\Gamma_\mathrm{b}\,\mathrm{d}t. \tag{41}$$

In our scheme this equality is trivially true for the first two equations but not for the momentum one. As a consequence, while the conservation of water and sediment volume is assured, shock-waves may numerically take place with a wrong speed and strength. This is an interesting feature, which becomes more important in long-term simulations, and is not, conversely, so significant in the corresponding cases over rigid bed.

The second property regards the behaviour of the approach when sediment transport vanishes. Only minor specifications are necessary to make the scheme working also in this limit situation. Firstly, it must be noticed that with $c = 0$ no sediment transport occurs and system (13) reduces to the classical shallow-water equations augmented with the fixed bed condition $\partial z_\mathrm{b}/\partial t = 0$. The number of waves of the RP does not change. Moreover, the speed of the second field vanishes: this means that bottom discontinuities do not evolve. The definition of $k_{i\pm1/2}$, employed in Eq. (33), is still valid if we pose any bed-discontinuity at a small distance ε on the right of the interface and we let $\varepsilon \to 0$. Finally, since flux function is discontinuous at the cell interface, we have to use the value in the limit position $x/t = 0^-$:

$$\mathbf{F}_{i+1/2} = \mathbf{F}(\tilde{\mathbf{U}}_{i+1/2}^n(0^-)). \tag{42}$$

The scheme resulting in this case is very similar to the one proposed by [10] for the fixed-bed case. Anyway, it is necessary to say that a mobile-bed solver could yield problems in the limit of fixed-bed. This is due to the particular wave-patterns that may take place in this case, i.e. the resonance phenomena faced by [1,10], which requires specific care in handling the solver. Solving these problems is by now beyond the scope of this paper.

An important fixed-bed situation is the steady condition of no fluid-motion over discontinuous bed topography. It is possible to show that the scheme satisfies the $\mathscr{C}$-property [6], provided that the solver gives the exact momentum flux. Let us consider the case of Fig. 4. In this situation the first wave-field is negative, the second is standing while the third one is positive; since no thrust is associate to the first and third field, it follows:

$$\mathbf{D}^{0,1} = \mathbf{D}^{2,3} = 0,$$
$$\mathbf{D}^{1,2} \neq 0.$$

Using Eq. (36), and assuming an exact solution for the RP, fluxes become:

$$\mathbf{F}_{i+1/2}^- = \mathbf{F}(\mathbf{U}_{i+1/2}^n(0^-)), \tag{43}$$
$$\mathbf{F}_{i+1/2}^+ = \mathbf{F}(\mathbf{U}_{i+1/2}^n(0^-)) + \mathbf{D}^{1,2}. \tag{44}$$

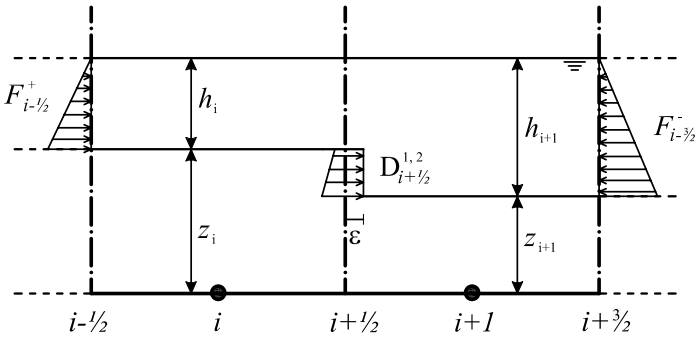

Fig. 4. Case of water at rest: scheme of the momentum fluxes around a bed-step.

In this situation the only flux components that are not null are the hydrostatic thrusts in the momentum expressions. Considering cell i, the side fluxes balance exactly, because $\mathbf{F}(\mathbf{U}^n_{i+1/2}(0^-))$ is the hydrostatic thrust associated to a depth h_1. For the cell $i+1$, the numerical flux $\mathbf{F}^+_{i+1/2}$ is the sum of the thrust of the fluid above the step and the thrust exerted by the step, and this sum balances exactly the flux $\mathbf{F}^-_{i+3/2}$. In these conditions the conserved variables do not change and the no-motion condition is preserved. In Section 5 we will show that the proposed solvers meet the requirement of giving the exact solution in this steady-state condition.

5. Three-wave Riemann solvers

The AWB scheme proposed in the previous section needs to specify the evaluation of the numerical fluxes as resulting from solution of RPs. Here, two approximate ways are presented. The first one assumes that the wave-fields are all shocks while, the second one, all rarefactions. Hereafter, for both situations, firstly we present a general approach, then we describe in detail the solvers for the geomorphic problem.

5.1. A three-shocks Riemann solver

The formulation of the three-shocks Riemann solver (3SRS) we are going to present shares the underlying philosophy that led to the well-known HLL solver [18] and can be considered as its natural extension. We consider here the case of a conservative PDE system composed by n equations, while in the next section a more general approach for a non-conservative system will be outlined. A short review of the HLL scheme is reported hereafter.

The HLL method assumes that the RP, despite its actual wave-composition, is constituted by a constant central state connected to the left and to the right states by shock waves. The unknowns of the RP problem are the speeds of the two shock waves, the n fluxes $\mathbf{F}$ and the n conserved variables $\mathbf{U}$ in the inner state. The total number of unknown is $2\times n+2$ and therefore, in order to solve exactly the problem, the same number of equations are needed. Available relations are the RH ones, which amount to $2\times n$, and n constitutive expressions, usually nonlinear, which relate fluxes to conserved variables in the inner state ($\mathbf{F}=\mathbf{F}(\mathbf{U})$). Solving the resulting nonlinear system can be a very expensive task. In the HLL approach, a way to approximate the solution is obtained with an explicit estimate (i.e. based only on the left and right known states) of the shock speeds. This choice reduces the number of unknowns to $2\times n$ and makes the RH relations linear in term of the n conserved variables and n fluxes. Now, since the number of reduced unknowns is equal to the number of RH equations, it is obvious to use them as the solving system, wiping out, in this way, the nonlinear $\mathbf{F}=\mathbf{F}(\mathbf{U})$ equations from the original set. The following well-known expression can therefore be obtained:

$$\mathbf{F}^{\mathrm{HLL}}=\frac{S^{1,2}\mathbf{F}^0-S^{0,1}\mathbf{F}^2+S^{1,2}S^{0,1}(\mathbf{U}^2-\mathbf{U}^0)}{S^{1,2}-S^{0,1}}. \tag{45}$$

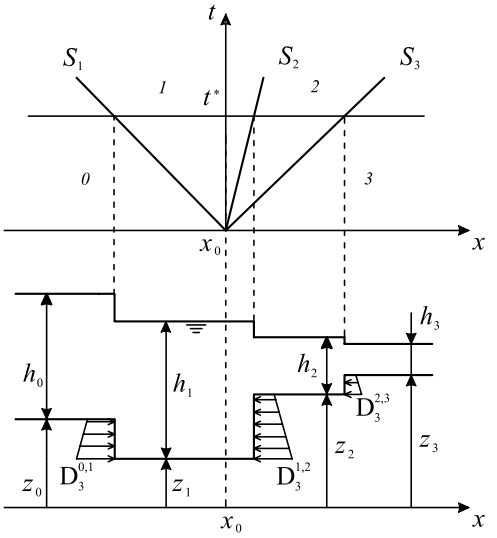

Fig. 5. Three-shocks configuration and associated pressure-thrusts in the 3RSS approximation at time $t = t^*$.

A key choice of the HLL approach concerns the estimates of the shock speeds; relevant information may be extracted from the eigenvalues of the system. Finally, it worths noticing that the nonlinear relations between conserved and primitive variables are fully kept in HLL approach.

In the 3SRS we assume that the RP, despite the actual wave composition, is constituted by two constant inner-states and three shock-waves (Fig. 5). The number of unknowns of the resulting RP are $4 \times n + 3$. Available relations are the $3 \times n$ RH expressions and $2 \times n$ nonlinear equations linking fluxes to conserved variables in the two inner-states. For $n = 3$ the number of equations are equal to the number of unknown while for $n > 3$ the number of equations exceeds the number of unknowns and therefore some relations must be disregarded. Again, as for the case with a single inner-state (as in HLL), whatever is $n \geqslant 3$, the solution of the resulting system may be overwhelmingly difficult. As in the HLL approach, a way to approximate the problem is to assume an explicit estimate of the shock speeds: the number of unknowns is reduced to $4 \times n$ and the $3 \times n$ RH relations become linear. Despite HLL, RH relations are anyway not sufficient to solve the problem, and n more equations must be provided. They must be chosen in the set $\mathbf{F} = F(\mathbf{U})$ in both the inner states. If these relations are linear, the resulting system is linear too, otherwise, as in the mobile-bed case, the resulting system becomes nonlinear and a specific method to deal with it must be used.

5.1.1. A three-shock Riemann solver for mobile-bed flows

Besides the question of solving a nonlinear system, another problem arises in the mobile-bed case: the RH relations (see Eq. (10)) present one more term respect the expressions deriving from conservative system of PDEs. Therefore, the linearization of the RH equations cannot be achieved simply assuming the value of the shock speed: also an estimate of the thrust term must be provided. The following explicit evaluation of the thrust may be obtained from the initial states of the RP:

$$\tilde{D}^{0,3} = g(c_j \Delta + 1)\left(h_j - \frac{|\zeta^{0,3}|}{2}\right)\zeta^{0,3}, \tag{46}$$

where $\zeta^{0,3} = z_0 - z_3$, $j = 0$ if $z_0 < z_3$ and $j = 3$ otherwise (see Fig. 5). Nevertheless, since the RP solution presents three thrust terms, it is necessary to make an assumption regarding the distribution of $\tilde{D}^{0,3}$ among the shocks.

To achieve accurate approximation of the RP solution in the framework of the 3SRS, we need, in the end, an algorithm to solve a nonlinear system, good estimation of the shock-speeds and the thrust term associated

to each wave. Since there is no direct way to pick up these quantities from the initial states, we suggest the following two-steps approach.

(1) First step

(a) *estimate of the shock speeds and the thrust terms:* for the shock speed we assume the following average

$$S^{i-1,i} = 0.5\left(\lambda_i^0 + \lambda_i^3\right), \quad i = 1,3, \tag{47}$$

where $[S^{0,1}\ \ S^{1,2}\ \ S^{2,3}]^{\mathrm{T}}$ is the vector of the shock speeds and $[\lambda_1^i\ \ \lambda_2^i\ \ \lambda_3^i]^{\mathrm{T}}$ is the vector of the eigenvalues evaluated in the ith zone. As far as the thrust term, we have verified that good results can be obtained giving the whole estimated thrust $\tilde{D}^{0,3}$ to $D_3^{1,2}$, i.e. the central shock, and therefore:

$$\mathbf{D}^{0,1} = \mathbf{D}^{2,3} = \begin{bmatrix} 0 \\ 0 \\ 0 \end{bmatrix}, \quad \mathbf{D}^{1,2} = \begin{bmatrix} 0 \\ 0 \\ \tilde{D}^{0,3} \end{bmatrix} \tag{48}$$

(b) *the system:* the system of 12 equations is composed by:

- the $3 \times 3 = 9$ RH relations (Eq. (10)) across each wave:

$$\mathbf{F}^i - \mathbf{F}^{i-1} - \mathbf{D}^{i-1,i} = S^{i-1,i}(\mathbf{U}^i - \mathbf{U}^{i-1}), \quad i = 1,3 \tag{49}$$

- two linear constitutive relations between fluxes and conserved variables:

$$U_3^1 = F_1^1 + \Delta F_2^1, \tag{51a}$$

$$U_3^2 = F_1^2 + \Delta F_2^2 \tag{51b}$$

- among the possible choices for the last constitutive equation, we have chosen the following one which leads to a solving system with the lowest degree of complexity:

$$F_2^1 = c_{\mathrm{b}}\beta\left(\frac{c_{\mathrm{b}}F_1^1 - F_2^1}{c_{\mathrm{b}}U_1^1 - U_2^1}\right)^3 \tag{52}$$

(c) *the solution:* the solution of the previous system has been obtained in the following way:

- at first, it is possible to solve analytically the reduced system made up of the 11 linear equations, obtaining, as solutions, linear functions of a chosen unknown, namely U_2^1; the coefficients of the polynomials depend only on the initial-state conserved variables (see Appendix A.4 for explicit expressions);
- the substitution of the obtained expressions in Eq. (52) gives rise to a polynomial of fourth degree in the unknown U_2^1 (see again Appendix A.4) that can be solved with well-known algorithms (see e.g. [30]). In general, the polynomial admits several solutions and therefore the right one must be picked up using some constraints (see e.g. [3]). We used the physical constraint that the total flux F_1^i and sediment flux F_2^i must have the same sign. An heuristic demonstration that this necessary condition is also sufficient comes from the convergence observed for all the several tests we performed.

(2) Second step

From the conserved variable obtained at the previous step, we evaluate the primitive variables in each inner state. Afterwards, the shock speeds are updated from an average of the corresponding eigenvalues

$$S^{i-1,i} = 0.5\left(\lambda_i^{i-1} + \lambda_i^i\right), \quad i = 1,3 \tag{53}$$

while the explicit estimate of the thrust associated to each wave ($D^{i-1,i}$, $i = 1,3$) is now available by Eq. (8) (see also Fig. 5). Finally, the points (b) and (c) of the first step are repeated, starting with the new values of the shock speeds and of the thrust terms. By doing so, the proposed solution of the RP considers the non-conservative flux in a somehow implicit way.

5.1.2. $\mathscr{C}$-property of the AWB scheme with the 3SRS solver

As explained in Section 4, in order to prove that the AWB scheme with 3SRS satisfies the $\mathscr{C}$-property, is sufficient to demonstrate that the condition of no fluid-motion over discontinuous bed topography (Fig. 4) is solution of the system solved by 3SRS in the first step. The second step is then skipped. It worths remembering that, in this situation, the momentum fluxes reduces to the hydrostatic thrusts.

Shock speeds evaluated with Eq. (47) give a Riemann structure in the x–t plane that is symmetric, with a vertical middle wave. The assumption with regard to the thrust terms (Eq. (48)) leads to the following RH relations:

$$\mathbf{F}^0 - \mathbf{F}^1 = S^{0,1}(\mathbf{U}^0 - \mathbf{U}^1), \tag{54a}$$

$$\mathbf{F}^2 - \mathbf{F}^3 = S^{2,3}(\mathbf{U}^2 - \mathbf{U}^3), \tag{54b}$$

$$\mathbf{F}^2 - \mathbf{F}^1 - \mathbf{D}^{1,2} = 0. \tag{54c}$$

The first two equations are obviously satisfied by the following constant solutions:

$$\begin{cases} \mathbf{F}^0 = \mathbf{F}^1, \\ \mathbf{U}^0 = \mathbf{U}^1, \end{cases} \quad \begin{cases} \mathbf{F}^2 = \mathbf{F}^3, \\ \mathbf{U}^2 = \mathbf{U}^3. \end{cases} \tag{55}$$

Moreover, they also satisfy the third one because $\mathbf{D}^{1,2}$ corresponds to the exact thrust term $\mathbf{P}$ which balances the momentum fluxes in no-motion condition. At last, these solutions satisfy automatically also the constitutive Eqs. (51) and (52). In other words, since the system solved by 3SRS in no-motion condition is exact, the solution is exact too.

5.1.3. LHLL as a simplified 3SRS

The theoretical framework we presented in the previous section can be used to show that the LHLL approach, presented in Section 3, is nothing but the AWB scheme with a very simplified version of the 3SRS. This helps to understand why LHLL may provide good results only in certain conditions.

The first assumption consists of setting the speed of the middle wave $S^{1,2}$ to zero. Therefore, it is clear that when this speed is significantly different from zero, the error may become significant. Moreover, the thrust terms $\mathbf{D}^{m-1,m}$ are evaluated as in the first step of the 3SRS, that is the total trust is assigned to the central wave. With this hypothesis, the set of equation deriving from the three RH conditions across the waves becomes, incidentally, equal to Eq. (54). To close this system, instead of using constitutive relations, the following equality between conserved variables in the two inner states is assumed:

$$\mathbf{U}^1 = \mathbf{U}^2. \tag{56}$$

This hypothesis is absolutely arbitrary, but renders the set of equation (Eqs. (54) and (56)) linear, whose solution is given by Eq. (25) with $\tilde{D}^{0,3}$ instead of $\tilde{\mathbf{H}}(z^n_{i+1} - z^n_i)$.

As far as the treatment of the non-conservative flux, we finally remark that both AWB and LHLL methods deal with it in an unsplitting way, but, whilst the latter is fully explicit, the former is somehow implicit.

5.2. A three-rarefaction Riemann solver for mobile-bed flows

In the literature, a number of Riemann solvers based on rarefaction waves has been proposed for different problems (see e.g. [9,12]). They assume that the RP is constituted by $n-1$ constant states, connected by n rarefactions, being n, as usual, the number of equations. In terms of primitive variables, the number of unknowns is $n\times(n-1)$, equal to the number n of primitive variables multiplied by the number $n-1$ of the inner constant-states. $(n-1)$ Riemann-invariants across each wave may be involved, so forming a set of $n\times(n-1)$ differential equations. The problem is therefore formally solvable but, because of its high non-linearity, it can be solved only with some linearization. The scheme we are going to present will be outlined for our case, where $n=3$, but can be plainly extended to problems with $n>3$. In the approach with three rarefaction-waves, named 3RRS, instead of Riemann invariants, we use the canonical equations, valid along

the characteristic lines, to connect the different constant-states. This choice has been suggested by preliminary tests, here unreported. Our approach is based on the following assumptions:

a. each rarefaction-fan collapses into a single line in the $\{x - t\}$ domain;
b. characteristic curves are assumed to be straight lines with a slope $\mathrm{d}x/\mathrm{d}t = 1/\tilde{\lambda}_j^{k,k+1}$, where $\tilde{\lambda}_j^{k,k+1}$ is a representative estimate of the jth eigenvalue in the rarefaction fan after the kth constant state.

This approach, when applied to cases with significant geomorphic evolution, has showed to yield not-enough accurate solutions if applied in one shot; therefore a two-step treatment has again, as in 3SRS, been exploited. In detail:

(1) Each point of a star zone (e.g., points 1 and 2 in Fig. 6a) can be connected to the left and right initial-data through the three characteristic-lines reaching it; using Eq. (24), the following two linear systems can be written:

$$\text{zone } 1 \begin{cases} \overline{\mathbf{C}}_1^{0,3} \cdot (\tilde{\mathbf{W}}^1 - \mathbf{W}^3) = 0, \\ \overline{\mathbf{C}}_2^{0,3} \cdot (\tilde{\mathbf{W}}^1 - \mathbf{W}^0) = 0, \\ \overline{\mathbf{C}}_3^{0,3} \cdot (\tilde{\mathbf{W}}^1 - \mathbf{W}^0) = 0, \end{cases} \tag{57}$$

$$\text{zone } 2 \begin{cases} \overline{\mathbf{C}}_1^{0,3} \cdot (\tilde{\mathbf{W}}^2 - \mathbf{W}^3) = 0, \\ \overline{\mathbf{C}}_2^{0,3} \cdot (\tilde{\mathbf{W}}^2 - \mathbf{W}^3) = 0, \\ \overline{\mathbf{C}}_3^{0,3} \cdot (\tilde{\mathbf{W}}^2 - \mathbf{W}^0) = 0, \end{cases} \tag{58}$$

where $\tilde{\mathbf{W}}^k$ is the vector of the primitive variables evaluated in zones $k = 1, 2$, and

$$\overline{\mathbf{C}}_i^{0,3} = \mathbf{C}_i\left(\frac{1}{2}(\mathbf{W}^0 + \mathbf{W}^3), \tilde{\lambda}_i^{0,3}\right), \quad \tilde{\lambda}_i^{0,3} = \frac{1}{2}(\lambda_i(\mathbf{W}^0) + \lambda_i(\mathbf{W}^3)) \tag{59}$$

(see (A.3) for the definition $\mathbf{C}_i(\mathbf{W}, \lambda)$). This step, which gives an approximate solution $\tilde{\mathbf{W}}$, can be considered as an application of the method of characteristics to the solution of a particular RP (see e.g. [24]).

(2) Starting from the approximated solution $\tilde{\mathbf{W}}$, it is possible to write two equations valid across each rarefaction wave (see Fig. 6b) obtaining the following linear system:

$$\begin{cases} \left.\begin{aligned} \overline{\mathbf{C}}_3^{01} \cdot (\mathbf{W}^1 - \mathbf{W}^0) = 0 \\ \overline{\mathbf{C}}_2^{01} \cdot (\mathbf{W}^1 - \mathbf{W}^0) = 0 \end{aligned}\right\} & \text{across } \lambda_1, \\ \left.\begin{aligned} \overline{\mathbf{C}}_1^{12} \cdot (\mathbf{W}^2 - \mathbf{W}^1) = 0 \\ \overline{\mathbf{C}}_3^{12} \cdot (\mathbf{W}^2 - \mathbf{W}^1) = 0 \end{aligned}\right\} & \text{across } \lambda_2, \\ \left.\begin{aligned} \overline{\mathbf{C}}_1^{23} \cdot (\mathbf{W}^3 - \mathbf{W}^2) = 0 \\ \overline{\mathbf{C}}_2^{23} \cdot (\mathbf{W}^3 - \mathbf{W}^2) = 0 \end{aligned}\right\} & \text{across } \lambda_3, \end{cases} \tag{60}$$

where

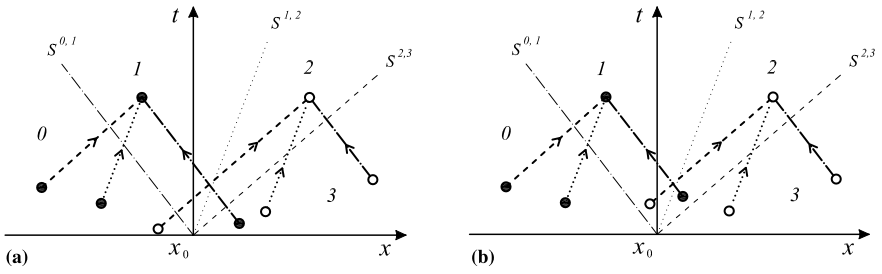

Fig. 6. Pattern of the characteristic lines in the (a) first iteration and (b) second iteration, employed in the 3RRS approximation.

$$\begin{cases} \overline{\mathbf{C}}_i^{m,m+1} = \mathbf{C}_i\left(\frac{1}{2}\left(\tilde{\mathbf{W}}^m + \tilde{\mathbf{W}}^{m+1}\right), \hat{\lambda}_i^{m,m+1}\right), \\ \hat{\lambda}_i^{m,m+1} = \frac{1}{2}\left(\lambda_i(\tilde{\mathbf{W}}^m) + \lambda_i(\tilde{\mathbf{W}}^{m+1})\right) \end{cases} \tag{61}$$

and $\tilde{\mathbf{W}}^0 = \mathbf{W}^0$, $\tilde{\mathbf{W}}^3 = \mathbf{W}^3$.

A remark is addressed to a specific feature of the canonical equations (60). Looking at the analytical expressions for $\overline{\mathbf{C}}_{i,3}^{m,m+1}$, with the help of Appendices A.3 and A.2, it is clear that these vectors take a reference pressure-value over the step equal to the average of the bottom pressure right uspstream and downstream of it. In order to be coherent with Eq. (8), it is necessary to substitute the previous expression with the corresponding reference-pressure deriving by Eq. (8) itself. The importance of this point will be stressed in the applications.

5.2.1. C-property of the AWB scheme with the 3RRS solver

As in the 3SRS case, in order to prove that the AWB scheme with 3RRS satisfy the $\mathscr{C}$-property, is sufficient to demonstrate that the condition of no-motion over discontinuous bed topography is solution of the system solved by the first step of the 3RRS. Second step is skipped in this situation.

Considering that $u_0 = u_3 = 0$, relations (59) give:

$$\tilde{\lambda}_1^{0,3} = \alpha, \quad \tilde{\lambda}_2 = 0, \quad \tilde{\lambda}_3 = -\alpha, \tag{62}$$

where $\alpha = 0.5(\sqrt{gh_0} + \sqrt{gh_3})$. Similarly, the coefficients of the systems (57) and (58) become:

$$\begin{bmatrix} C_{1,1} = -g\tilde{h}\alpha \\ C_{1,2} = -\tilde{h}\alpha^2 \\ C_{1,3} = -\tilde{k}\alpha \end{bmatrix}, \quad \begin{bmatrix} C_{2,1} = 0 \\ C_{2,2} = 0 \\ C_{2,3} = 0 \end{bmatrix}, \quad \begin{bmatrix} C_{1,1} = g\tilde{h}\alpha \\ C_{1,2} = -\tilde{h}\alpha^2 \\ C_{1,3} = \tilde{k}\alpha \end{bmatrix},$$

where $\tilde{h} = 0.5(h_0 + h_3)$. System (57) reduces to the following two equations:

$$\begin{aligned} -\alpha(h_1 - h_3) - \alpha^2(u_1) - \alpha(z_1 - z_3) = 0, \\ \alpha(h_1 - h_0) - \alpha^2(u_1) + \alpha(z_1 - z_0) = 0 \end{aligned} \tag{63}$$

which sum to:

$$-\alpha(2\alpha u_1 + h_0 - h_3 + z_0 - z_3) = 0. \tag{64}$$

Considering the condition of horizontal free-surface, i.e. $h_0 + z_0 = h_3 + z_3$, $u_1 = 0$ is solution to the previous expression. Furthermore, considering that in no-motion condition the bed elevation cannot change, it must be $z_1 = z_0$; as a consequence, $h_1 = h_0$ is solution of (63). Similarly, we end up with $u_2 = 0$, $z_2 = z_3$ and $h_2 = h_3$ in the second inner-state.

6. Numerical tests

In this section the solutions of a series of test cases, obtained with both the AWB and LHLL schemes, will be presented. The first group of tests are Riemann problems for the movable-bed equations (5), in which the bottom shear-stress has been neglected in the momentum equation. The relevant exact solutions have been worked out by a process of subsequent wave-field construction, starting from either initial-state (left or right), and coming to define, in the end, the other one. In so doing an inverse problem is solved in the way outlined by [2,13].

The second group of tests regards a case of practical interest in the field of river engineering, that is the evolution of a trench, initially dug in the bed, in both subcritical and supercritical conditions. The system (5) is here solved including also the effect of the friction force on the bottom. In these applications wave interactions and friction effects make the flow more complex, and no relevant exact solution is available; therefore we could just compare the results of AWB with LHLL.

Beyond their importance in assessing the numerical properties of the schemes, all the test cases have been chosen also to highlight the role of the morphological changes on the flow when the sediment transport is very high, or massive, as in debris flows.

6.1. Riemann problems

We are going to present two different RP tests selected to stress the different behaviour of AWB and LHLL against exact solutions. Initial conditions are shown in Table 1. To be consistent with the thrust calculation in the exact solutions, LHLL has been here applied substituting, in Eq. (25), the term $\tilde{\mathbf{H}}(z^n_{i+1} - z^n_i)$ with an explicit evaluation of $\mathbf{D}$ obtained from the initial states of the local RP (see Eq. (46)). In this way, LHLL uses the same evaluation of the thrust term used in the first step of the AWB-3SRS approach. All the simulations make use of the CFL coefficient equal to 0.95.

Test A. The Riemann problem with data reported in Table 1, Test A, is now considered. The relevant self-similar solution is composed by two external rarefaction-waves and a central shock (Fig. 7). The shock is moving slowly, compared with the other two waves, and absorbs most of the initial step in bed profile.

Although convergent, LHLL solution (Fig. 7a) does not capture the shock, which is smoothed out, and shows there the biggest deviations from the exact solution, at $t = 2$ s. This mismatch is more and more pronounced as time passes, as it can be inferred from Fig. 8a, which reports the numerical solution at time $t = 20$ s, in a reference system moving with the shock speed. The result points out a strong numerical diffusion, arising from a poor representation of the intercell solution of the RP. In fact, the numerical fluxes at the intercell border and those calculated with the primitive variables at the center cell exhibit a remarkable difference around the central wave, as shown in Fig. 9a. It must be said that in this test the limiter for the solid-mass discharge (Eq. 26) never switches on.

On the contrary, the two AWB schemes yield almost undistinguishable solutions, able to capture the central wave (Fig. 7b) not only at $t = 2$ s but also as time passes, as shown in Fig. 8b. The shock is well captured but not perfectly positioned. This outcome is not a trace of leaks in the mass conservations, which is indeed exactly satisfied at any time. The intimate cause of this error is linked to the approximation of the non-conservative flux, as explained in Section 4, which leads to a small error in the shock speed. The delay between numerical and exact shock-position becomes, of course, more important in long-term simulations. As far as the comparison between cell-centered and intercell fluxes is concerned, Fig. 9b shows a remarkable consistency (while LHLL produced a clear mismatch), although some deviations from the exact values are present, being the methods employed at a low order of accuracy.

A further comment is addressed to the 3RRS skill to model different expressions for the thrust term, as described in Section 5.2, and the effect they have on the solution. We consider a test as type A, but with a slight increment of the initial bed-step, so to enhance the effect under examination. Fig. 10 depicts the effect of different evaluations of the bottom thrust on the flow, which is clearly not negligible.

Test B. The RP with data in Table 1, Test B, is here considered. The relevant self-similar solution is composed, from left to right, by two-rarefaction waves and a shock (Fig. 11). The central wave is a quite-slowly moving rarefaction, bearing most of the initial step of the bed profile, whereas the shock is very weak, almost ineffective for the bed.

In this test the LHLL solutions are affected by the limiter (Eq. (26)). Switching it off, the solution has a very smeared bed-profile in the central rarefaction (Fig. 11a). Again, as in Test A, this diffusive behaviour attends differences between the fluxes evaluated in the middle and at the intercell side of the cells; Fig. 12a illustrates this point around the central rarefaction for the solid-mass discharge, the least accurate flux in the numerical solution. The numerical flux displays a very different behaviour respect the exact one, reaching even negative values. This situation is completely unphysical, because liquid and solid discharges have to move accordingly with the mixture velocity u. LHLL results obtained with the limiter are presented in Fig. 11b. They are less diffusive and have smaller errors than the companion solution without the limiter. Fig. 13a illustrates the

Table 1
Initial values for the test cases

Test A			Test B		
(m)	(m/s)	(m)	(m)	(m/s)	(m)
$h_L = 2.00$	$u_L = 1.00$	$z_L = 3.00$	$h_L = 6.00$	$u_L = 0.01$	$z_L = 1.00$
$h_R = 5.00$	$u_R = 3.54$	$z_R = 1.14$	$h_R = 0.38$	$u_R = 5.01$	$z_R = 3.75$

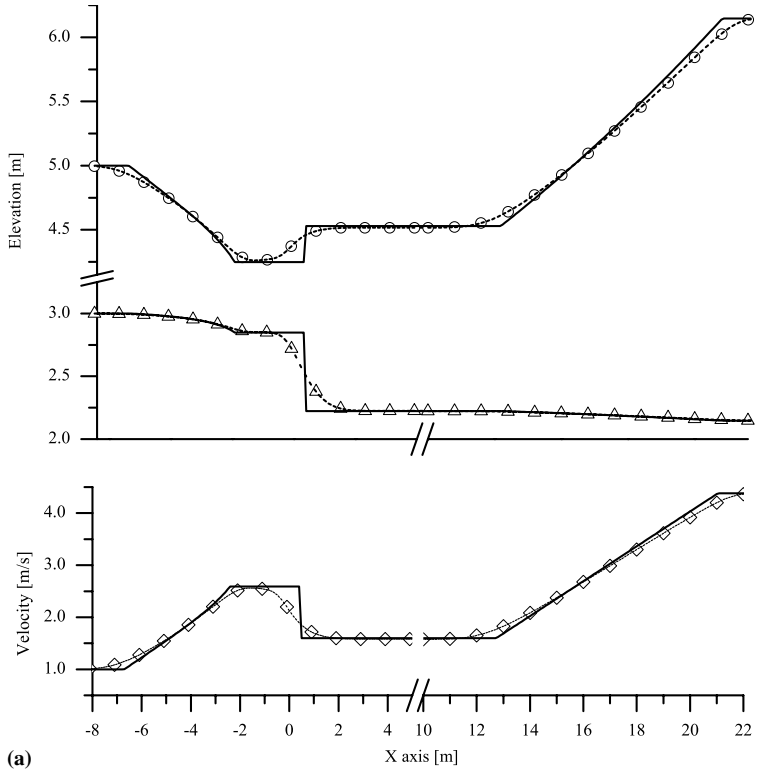

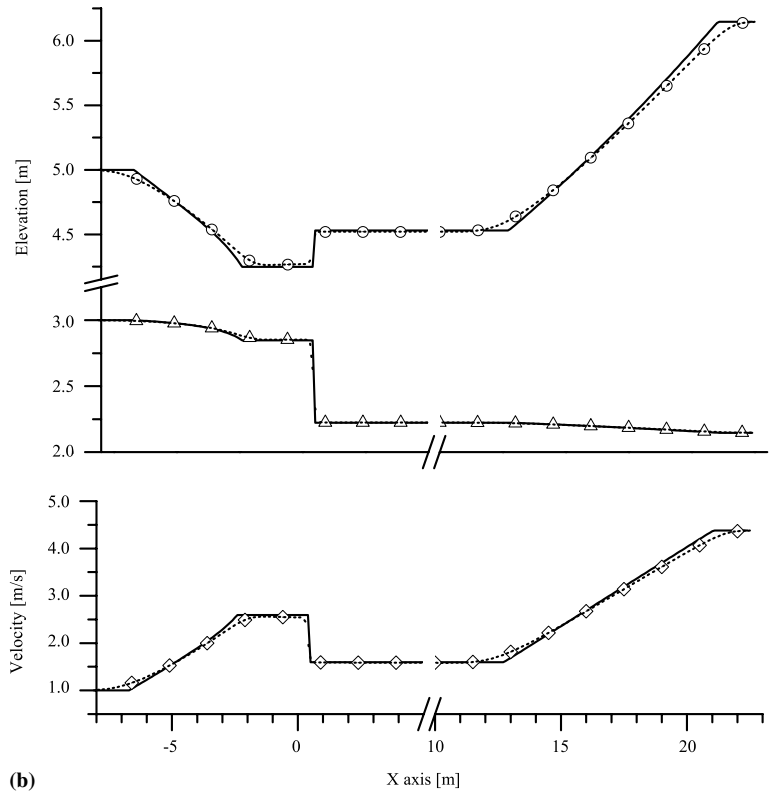

Fig. 7. Test A: evaluation of free-surface (⊙), bed profile (△) and velocity (◇) at $t = 2$ s and with $\Delta x = 0.1$ m. Comparison between exact solution (—) and result of: (a) LHLL, (b) AWB-(3SRS, 3RRS).

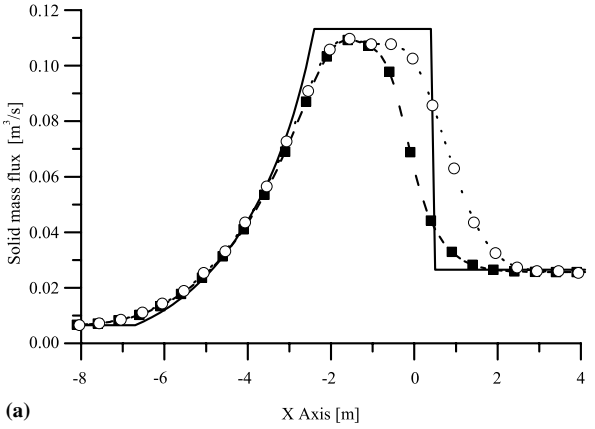
0.12
0.10
0.08
0.06
0.04
0.02
0.00
Solid mass flux [m²/s]
-8
-6
-4
-2
0
2
4
X Axis [m]

(a)

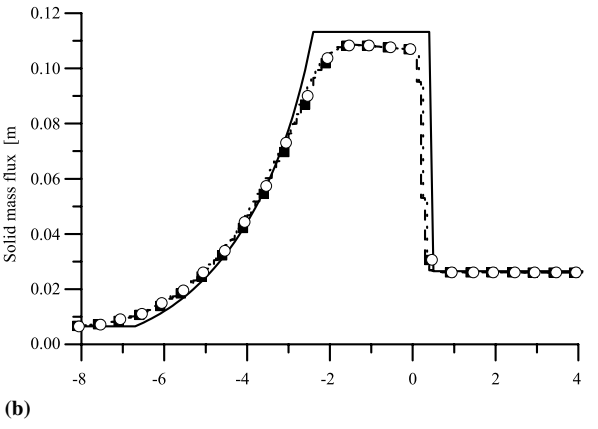
0.12
0.10
0.08
0.06
0.04
0.02
0.00
Solid mass flux [m
-8
-6
-4
-2
0
2
4

(b)

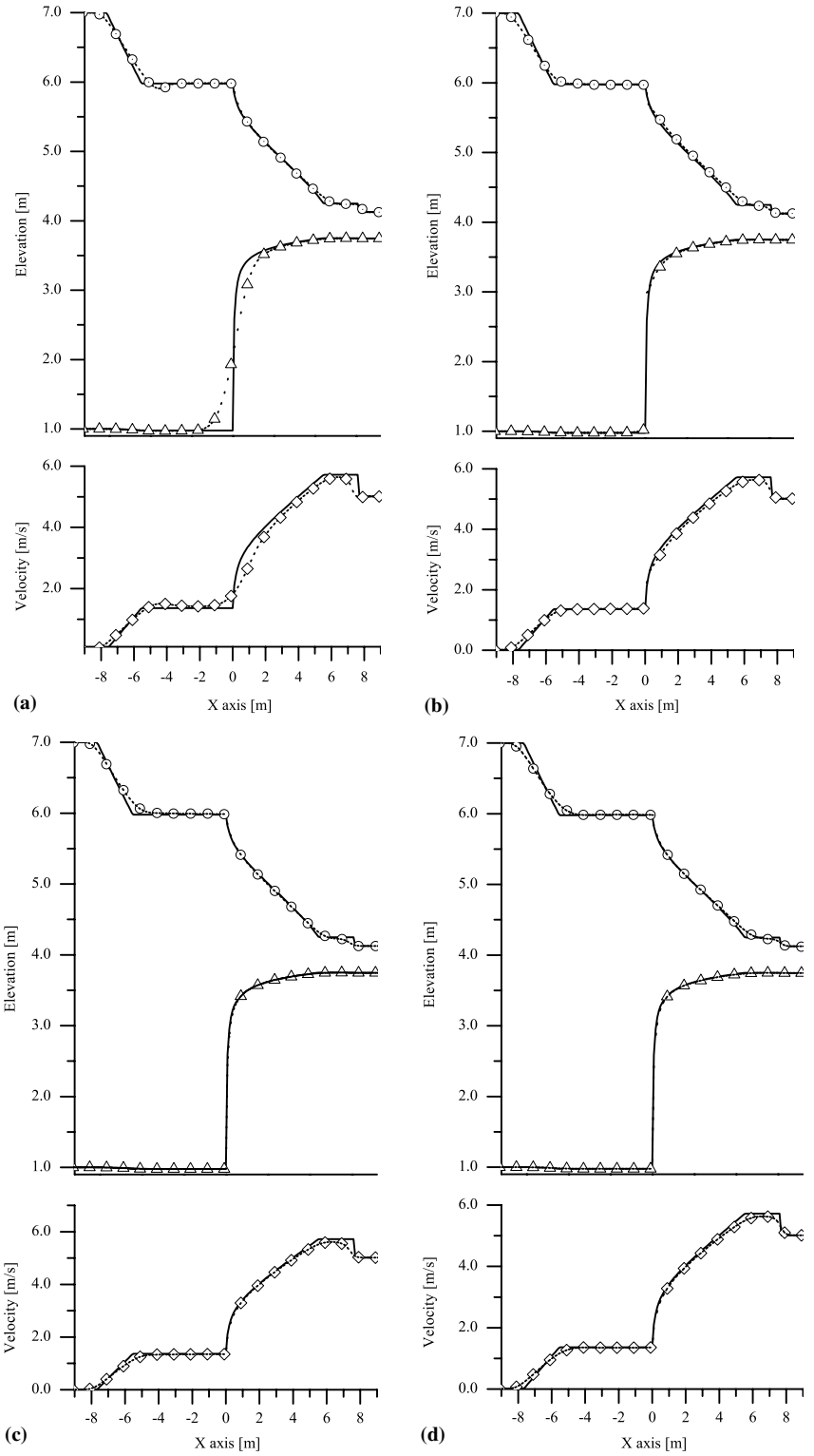

Fig. 11. Test B: evaluation of free-surface (⊙), bed profile (△) and velocity (◇) at $t = 1$ s and with $\Delta x = 0.1$ m. Comparison between exact solution (—) and results of: (a) LHLL without limiter, (b) LHLL with the limiter, (c) AWB-3SRS, (d) AWB-3RRS.

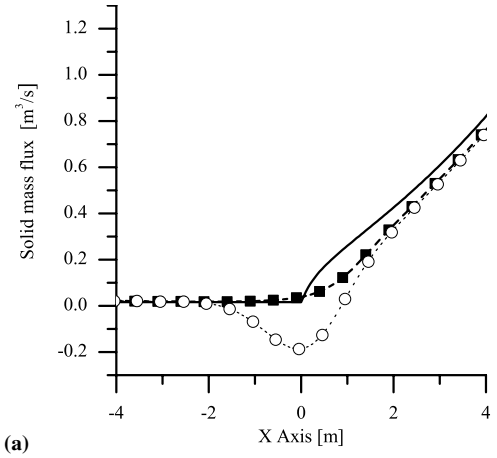

(a)

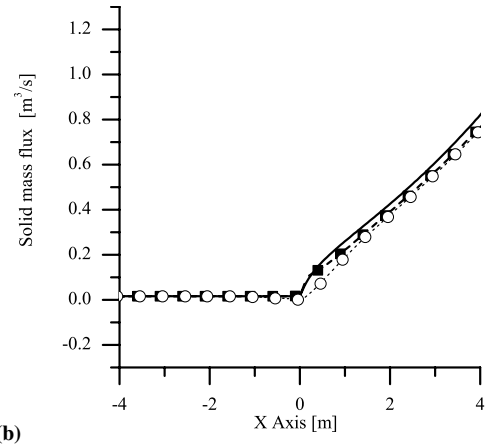

(b)

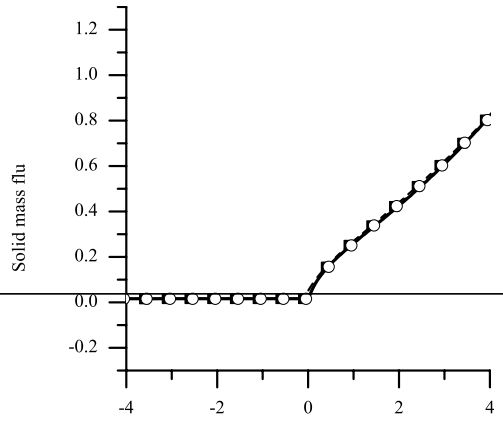

(c)

bed profiles, at $t = 30$ s, around the middle wave, including both the solutions obtained with and without the limiter. It may be noticed that the solution with the limiter presents a central field shaped as a compound wave, formed by a piece of shock with, on either side, two pieces of rarefactions. This particular and wrong wave pattern is present also at the early stage of the flow, although, as observed at $t = 1$ s (see Fig. 11b), it cannot be appreciated. As time passes, the strength of the central shock reduces more and more and the

solution tends to the extremely diffusive one obtained without the limiter: in the long run, the limiter ceases to be effective on the solution. This behaviour is almost independent on the grid refinements.

Numerical solutions of the two AWB versions are quite similar and fit rather well the exact one, including the central rarefaction-wave, where the LHLL, with and without the limiter, failed. In Figs. 11c and d, the graph of the primitive variables is sketched at time $t = 1$ s: apparently very small differences may be appreciated between the AWB solutions and the LHLL(+limiter) one. Nevertheless, at a careful inspection, fluxes present different values around the middle rarefacion, as shown in Figs. 12b–d. These differences are responsible of the fact that, as time passes, while the AWB solutions keep a good description of the rarefaction (Fig. 13b), the LHLL ones degenerate (Fig. 13a). After this comparison, it may be inferred that the proposed AWB method is qualified to predict good solutions also on long term, till the unsteady character of the RP solutions above considered is damped out. These cases offer, once more, a sharp impression on how sensitive is the numerical prediction of shallow-water flows over movable bed. Small changes in the numerical strategy, as switching on/off the limiter in the LHLL method, may yield sensible variations, at least at the early stages. AWB, on the whole, appears to give sound answers to all the Riemann tests exhaminated, for short and long times. Same overall behaviours have been observed in several other tests, performed but not here reported for sake of brevity.

6.2. Evolution of a trench

The tests presented in this section regard the evolution of a trench dug in river bed. The trench has been schematized as a big cavity in the bed with assigned geometry (Fig. 14). Essentially it has a trapezoidal shape and a straight bed line with the same slope of the external domain. The initial banks of the trench are very steep. To sort out the effects on the flow induced by the trench, both reaches upstream and downstream of it are supposed to be in steady uniform conditions and long enough to make boundary conditions not influential. The flow is strongly unsteady after the start, and then it develops toward asymptotic uniform conditions. As the flow evolves, the bottom friction term plays a fundamental role and is therefore kept in the model. Its local value has been computed by means of the Chézy formulation,

$$\frac{\tau}{\rho_w} = \frac{g}{\chi} u^2 \tag{65}$$

being χ ($m^{1/2}/s$) the Chézy friction factor. To discretize this term a standard splitting technique for source terms is adopted. The ODE of the source problem ($d\mathbf{U}/dt = \mathbf{S}(\mathbf{U})$) associated to system (5) is solved by an implicit Euler scheme. Details of this approach can be found in [14].

Initial conditions consist, on either side of the trench, of the uniform flow depth h_0 and velocity U_0 given in Table 2. The bed slope is consistent with Eq. (65), while the other parameters in the table allow to calculate the sediment transport and the sediment concentration in the same uniform reaches. In the trench it is initially imposed a volumetric discharge equal to $U_0 h_0$, and a straight free-surface line tilted with slope i_f and aligned with the free-surface outside the trench; the flow depth is therefore initially greater in the trench, and the velocity, as a consequence, smaller.

It is expected that waves soon arise from the two banks of the trench and, after a short time, interact each other giving rise to compound structures: some of them run the flow domain toward the upstream end, the remainder ones toward the downstream end. Amplitudes and speed of these compound waves are not the same, and depend both on the trench geometry and the features of the basic uniform flows, in particular

Table 2
Values of physical variables and parameters employed in the trench-evolution test

		Subcritical condition	Supercritical condition
Fr	Froude number	0.85	1.2
i_f	Bed slope	8.83×10^{-3}	1.57×10^{-2}
χ	($m^{1/2}/s$)	28.32	29.88
β	($m^{1/2}/s$)	1×10^{-4}	5×10^{-4}
h_0	(m)	2.	2.
U_0	(m/s)	3.76	5.31

on the Froude number. For a specific analysis of this topic we address to [24]. Because of the above considerations, we decided to simulate two different situations, the first one with a subcritical uniform flow ($Fr < 1$), the second one with a supercritical uniform flow ($Fr > 1$).

All the following numerical simulation has been performed using cell width $\Delta x = 0.05$ m and CFL coefficient equal to 0.95.

6.2.1. Supercritical condition

In this test the trench is 2 m long, 0.9 m deep and the slope of the trench banks is equal to 5. Fig. 14 presents the numerical evolution of the bed profile at two different times, obtained with the different methods. Because of the supercritical condition, the presence of the trench induces significant effects both upstream and downstream along the torrent. The snapshot shows two separate wave structures forming on the bed. Between the two, a piece of almost flat bed-profile takes place, which remains below the original level of the bed at the two upper edges of the trench. The wave structure moving downstream is quite strong at the first time, and becomes weaker at the subsequent observation. On the contrary, the trough-shaped bed-wave moving upstream reduces its strength, as time passes, at a much smaller rate. This behaviour, somehow surprising, is reminiscent of the way bedforms called antidunes evolve in a river bed. Comparing the results of the two methods, LHLL is more diffusive than AWB and clear differences affect both the bed-wave structure and the region in between. As time passes these differences are reducing, also because the bottom friction source term becomes more and more influencing the outcome. The asymptotic uniform flow condition is expected, in fact, to be the same for the two methods.

6.2.2. Subcritical conditions

The trench is 2 m long, 0.6 m deep and the slope of the sides is equal to 5. Fig. 15 presents the numerical evolution of the bed profile at two different times, obtained with the different methods. Opposite to the case previously described, the present subcritical conditions determine (or should, at least theoretically) major downstream effects, whereas in the upstream direction just small perturbations on the bed propagate. Relying on AWB results, the snapshot shows that the upstream bank of the trench moves downstream very slowly, and

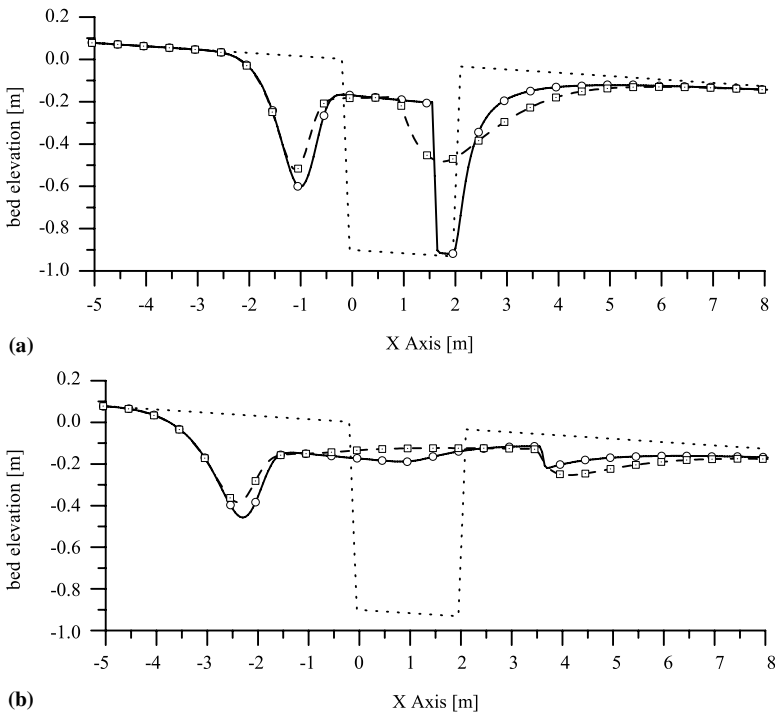

Fig. 14. Evolution of an initial trench (···) in supercritical conditions: numerical solution obtained, at (a) $t = 10$ s, (b) $t = 20$ s, with (⊡) LHLL and (○) AWB-3SRS.

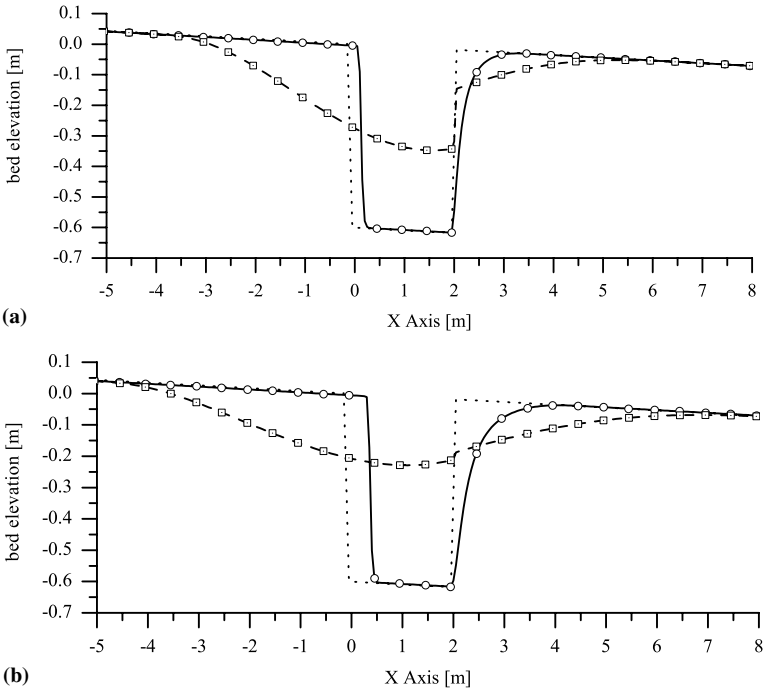

Fig. 15. Evolution of an initial trench (···) in subcritical conditions: numerical solution obtained, at (a) $t = 30$ s, (b) $t = 60$ s, with (⊡) LHLL and (○) AWB-3SRS.

keeps its steepness; the downstream bank of the trench is displacing in the flow direction with a shape which is milder at later times, resembling a rarefaction curve. The bottom of the trench moves and reduces, but remain, this time, perfectly overlapping to the original one. A similar behaviour is experimentally and numerically observed by [23]. Comparing the results of the two methods, LHLL strongly diffuses around the upstream bank, triggering an unphysical wave spanning also in the domain upstream of the initial trench position. The downstream bank of the trench is developing the strange compound wave already described in Section (6), dealing with the RP test B. This wave has a central discontinuous core, which is swept away at longer times, as visible in Fig. 15, too. All considered, differences in the numerical results by the two methods are more impressive in this sub-critical case, where they also last longer.

7. Conclusions

In this paper the rapid transients of shallow water flows over an erosional bed have been considered. The material entrainment from the bed creates a strong interaction with the free-surface current, resulting in the possible formation of strong and weak shocks. Their simulations demand for a formulation of a mathematical model able to handle the geomorphic behaviour.

A new numerical model has been here proposed, a finite volume method based on a Godunov-type evaluation of the fluxes. It represents an extension to the case of movable bed of a well-balanced technique already proposed for shallow water flows over rigid bed with topographical indentations. This new scheme, named AWB, looks for an approximated solution of the intercell RP. We developed new RP-solvers which deploy the complete wave-structure, keep the coupling between bed and flow dynamics and, without any split, embody the effect of the non-conservative pressure-thrust on the bottom. This procedure is worked out into two steps, so to achieve a degree of implicitness in the treatment of the non-conservative term.

To assess the skill of the new scheme, we compared the numerical results with new exact solutions of Riemann problems. In addition, applications to cases of practical interest have been considered, where the friction forces on the bed are taken into account. Along with the new AWB method, we also applied, to the same test cases, an existing Godunov-type method, named LHLL, based on the same mathematical model.

Results for AWB are quite satisfying. The new method works well in both the RPs and in the applicative tests. Simple and compound waves are well predicted at the different stages of the solution, without significant spurious diffusion and inaccuracy. Comparisons with LHLL results, which show significant limits, allow to understand the importance of the well-balanced calculation of the fluxes and of the implicit, unsplit evaluation of the non-conservative term in AWB.

The new method has been here presented at the first-order of accuracy to assess the substantial improvement due to the novel key-features introduced. A second-order version can be straightforwardly obtained by MUSCL-Hancock technique, following [14]. The results make it promising to be applicable also to real situations, where, beyond the many sources of complexity, there is a more stringent demand for accuracy in predicting the morphological evolution, which must be followed for long time.

Acknowledgement

Authors wish to thank M. Giuliani for the precious help in developing the codes and in running the test used in this paper and E. Casagrande for the help in sketching the figures. This work has been funded by a joint IMONT (Istituto Nazionale della Montagna, Italy) and PAT (Provincia Autonoma di Trento) Project.

Appendix A

A.1. Summary of the notation used in this paper

Variables in a RP are defined both *inside* the constant-value zones and *across* the waves that connect two constant states; moreover they may be associated to an eigenvalue; at last, because of the self-similarity of the solution, they are time-independent and no explicit indication about time is needed. Therefore, the following notation has been assumed:

$\mathbf{\Omega}^n$ $\iff$ vector variable evaluated in the nth *zone of a RP*
Ω_j^n $\iff$ jth component of a vector variable evaluated in the nth zone of a RP
$\mathbf{C}_i$ $\iff$ vector variable associated to the ith eigenvalue of a RP
$C_{i,j}$ $\iff$ jth component of a vector variable associated to the ith eigenvalue of a RP
$\mathbf{\Psi}^{n,m}$ $\iff$ vector variable defined across zone m and n of a RP
$\Psi_j^{n,m}$ $\iff$ jth component of a vector variable defined across zone m and n of a RP
$\mathbf{\Psi}_{i\pm1/2}^{n,m}$ $\iff$ vector variable defined across zone m and n of a RP located at at $x = i \pm 1/2$.

Moreover, the following equivalences has been set:

$$k = gh(c\Delta + 1), \quad r = qg + 2,$$
$$q = \beta c_b \Delta, \quad s = \frac{1}{2} r u^2 + gh.$$

A.2. Characteristic polynomial

The characteristic polynomial deriving from (18) is:

$$\alpha_3 \lambda^3 + \alpha_2 \lambda^2 + \alpha_1 \lambda + \alpha_0 = 0,$$

where

$$\alpha_3 = h + u^2(2\beta + 3q),$$
$$\alpha_2 = -qu(7u^2 + g(\beta u^2 + h)) + u\beta\left(-5u^2 + 2gh\left(\frac{k}{h} - 1\right)\right) - 2uh,$$
$$\alpha_1 = \frac{1}{2} q u^2((8 + 3\beta g)u^2 + gh) - \beta u^2\left(-3u^2 + gh\left(5\frac{k}{h} - 3\right)\right) - h(gh - u^2),$$
$$\alpha_0 = 3kg\beta u^3.$$

A.3. Coefficients of the linearized characteristic equations

Coefficients of the linearized characteristic equation (24) are expressed by the following relations:

$$C_{i,1}(\mathbf{W},\lambda_i) = \left(-\frac{1}{2}qu^2 - h\right)g\lambda_i,$$
$$C_{i,2}(\mathbf{W},\lambda_i) = 2\left(\frac{\lambda_i}{c_\mathrm{b}}(s-\lambda_i u) + \frac{u-\lambda_i}{c_\mathrm{b}}k\right)\beta c_\mathrm{b}u + (u-\lambda_i)\lambda_i(3qu^2+h),$$
$$C_{i,3}(\mathbf{W},\lambda_i) = (u-\lambda_i)k.$$

A.4. Quartic polynomial of the 3SRS for the mobile-bed case

In this appendix, we give the expression of the terms available after the solution of the linear part of the 3SRS system and which are then used in Eq. (52). Moreover, we will give the expression of the terms of the quartic polynomial of the 3SRS. Setting

$$\alpha = \frac{1}{(-S_L+S_{12})(S_R-S_L)}, \quad \mu = \frac{-\Delta(-S_L+S_R)(-S_L+S_{12})}{(-S_L+S_{12})(S_R-S_L)},$$
$$D_\mathrm{tot} = D_{12}+D_{01}+D_{21}$$

we have:

$$F_1^1 = ax+b, \quad F_2^1 = cx+d, \quad U_1^1 = ex+f,$$

where

$$a = \mu S_L,$$
$$b = \alpha\{S_R S_{12}F_{01} + S_L^2(-U_{02}\Delta(S_{12}-S_L+S_R)+U_{03}) + S_L[\Delta F_{02}(S_{12}-S_L+S_R) - S_{12}(F_{31}+\Delta F_{32}) + F_{33}-F_{03}] - S_L S_R(S_{12}(-U_{31}+U_{01}+\Delta U_{32})+U_{33}) + S_L D_\mathrm{tot}\},$$
$$c = S_L,$$
$$d = F_{02} - U_{02}S_L,$$
$$e = \mu,$$
$$f = \alpha\{-F_{03}+F_{33}+F_{01}(S_{12}-S_L+S_R) + \Delta F_{02}(S_{12}-S_L+S_R) - S_{12}(F_{31}+\Delta F_{32}) + S_R S_{12}(U_{31}+\Delta U_{32}) - S_R U_{33} - S_L((U_{01}+\Delta U_{02})(S_{12}-S_L+S_R)-U_{03}) + S_L D_\mathrm{tot}\}.$$

The quartic polynomial in $U_2^1 = x$ is:

$$\rho_4 x^4 + \rho_3 x^3 + \rho_2 x^2 + \rho_1 x + \rho_0 = 0,$$

where:

$$\rho_4 = c(c_\mathrm{b}e-1)^3,$$
$$\rho_3 = c_\mathrm{b}ed(3+ec_\mathrm{b}(ec_\mathrm{b}-3)) + 3c_\mathrm{b}fc(ec_\mathrm{b}-1)^2 + 3\beta c_\mathrm{b}^2 ac(c_\mathrm{b}a-c) + c_\mathrm{b}\beta(c^3 - c_\mathrm{b}^3 a^3) - d,$$
$$\rho_2 = 3\left[-\frac{1}{2}\beta c_\mathrm{b}^3 ab(2c_\mathrm{b}a-c) + ec_\mathrm{b}^2 f(c_\mathrm{b}fc + d(ec_\mathrm{b}-2)) - \beta dc_\mathrm{b}c(2c_\mathrm{b}a-c) + c_\mathrm{b}f(-c_\mathrm{b}fc+d) + \beta c_\mathrm{b}^2(a^2dc_\mathrm{b} - c^2b)\right],$$
$$\rho_1 = 3\left[\beta c_\mathrm{b}^3 ab(2d-c_\mathrm{b}b) - \beta d^2 c_\mathrm{b}(c_\mathrm{b}a-c)c_\mathrm{b}^2 f^2\left(\frac{1}{3}c_\mathrm{b}fc + d(ec_\mathrm{b}-1)\right) - \beta c_\mathrm{b}^2 bc(2d-c_\mathrm{b}b)\right],$$
$$\rho_0 = -3\beta dc_\mathrm{b}^2 b(d-c_\mathrm{b}b) + c_\mathrm{b}d(\beta d^2 + c_\mathrm{b}^2 f^3) - c_\mathrm{b}^4\beta b^3.$$

References

[1] F. Alcrudo, F. Benkhaldoun, Exact solutions to the Riemann problem of the shallow water equations with a bottom step, Comput. Fluids 30 (2001) 643–671.
[2] N. Andrianov, Performance of numerical methods on the non-unique solution to the Riemann problem for the shallow water equations, Int. J. Numer. Meth. Fluids 47 (2005) 825–831.
[3] N. Andrianov, G. Warneckle, On the solution to the Riemann problem for the compressible duct flow, SIAM J. Appl. Math. 64 (3) (2004) 878–901.
[4] A. Armanini, H. Capart, L. Fraccarollo, M. Larcher, Rheological stratification in experimental free-surface flows of granular liquid mixtures, J. Fluid Mech. 532 (2005) 269–319.
[5] K. Ashida, M. Michiue, Study on hydraulic resistance and bedload rate in alluvial streams, Trans. Jpn. Soc. Civil Eng. 206 (1972) 59–69.
[6] A. Bermudez, M.E. Vázquez, Upwind methods for hyperbolic conservation laws with source terms, Comput. Fluids 23 (1994) 1049–1071.
[7] Z. Cao, G. Pender, S. Wallis, P. Carling, Computational dam-break hydraulics over erodible sediment bed, J. Hydraulic Eng. 130 (7) (2004) 689–703.
[8] H. Capart, D.L. Young, Formation of a jump by the dam-break wave over a granular bed, J. Fluid Mech. 372 (1998) 165–187.
[9] C.E. Castro, E.F. Toro, A Riemann solver and upwind methods for a two-phase flow model in non-conservative form, Isaac Newton Institute for Mathematical Sciences, Preprint Series, no. NI05001-NPA, 2005.
[10] A. Chinnayya, A.-Y. LeRoux, N. Seguin, A well-balanced numerical scheme for the approximation of the shallow-water equations with topography: The resonance phenomenon, Int. J. Finite Volumes (2004).
[11] N. Črnjarić-Žic, S. Vuković, L. Sopta, Extension of ENO and WENO schemes to one-dimensional sediment transport equations, Comput. Fluids 33 (2004) 31–56.
[12] W. Dai, P.R. Woodward, An iterative Riemann solver for relativistic hydrodynamics, SIAM J. Sci. Comput. 14 (4) (1997) 982–995.
[13] L. Fraccarollo, H. Capart, Riemann wave description of erosional dam-break flows, J. Fluid Mech. 461 (2002) 183–228.
[14] L. Fraccarollo, H. Capart, Y. Zech, A Godunov method for the computation of erosional shallow water transient, Int. J. Numer. Meth. Fluids 41 (9) (2003) 951–976.
[15] S.K. Godunov, Finite difference method for numerical computation of discontinuous solution of the equations of fluid dynamics, Mat. Sb. 47 (1959) 271–300.
[16] J.M. Greenberg, A.-Y. LeRoux, A well-balanced scheme for the numerical processing of source terms in hyperbolic equations, SIAM J. Numer. Anal. 33 (1996) 1–16.
[17] A. Harten, B. Engquist, S. Osher, Chakravarthy, Uniformly high order accuracy essentially non-oscillatory schemes III, J. Comput. Phys. 71 (1987) 231–303.
[18] A. Harten, P.D. Lax, B. Van Leer, On upstream differencing and Godunov-type schemes for hyperbolic conservation laws, SIAM Rev. 25 (1983) 35–61.
[19] E. Isaacson, B. Temple, Convergence of the 2×2 Godunov method for general resonant nonlinear balance law, SIAM J. Appl. Math. 55-3 (1995) 625–640.
[20] R.J. LeVeque, Numerical Methods for Conservation Laws, second ed., Birkhäuser, Basel, 1992.
[21] E. Meyer-Peter, R. Müller, Formulas for bed-load transport, in: Proc. of 2nd Meeting IAHSR, Stockolm, Sweden, 1948. pp. 1–26.
[22] P.H. Morris, D.J. Williams, Relative celerities of mobile bed flows with finite solids concentrations, J. Hydraulic Eng. 122 (1996) 311–315.
[23] L. van Rijn, Sedimentation of dredged channels by currents and waves, J. Waterway Port Ocean Eng. 2 (5) (1986).
[24] G. Rosatti, L. Fraccarollo, A. Armanini, Behaviour of small perturbations in 1d mobile-bed models, in: R. Della Morte, M. Greco, A. Carravetta (Eds.), RiverFlow 2004, Balkema, The Netherlands, 2004.
[25] B.M. Sumer, A. Kozakiewicz, J. Fredsøe, R. Deigaard, Velocity and concentration profiles in sheet-flow layer of movable bed, J. Hydraulic Eng. 122 (1996) 549–558.
[26] T. Takahashi, Debris Flow, Balkema, The Netherlands, 1991.
[27] V.A. Titarev, E.F. Toro, ADER: arbitrary high order Godunov approach, J. Sci. Comput. 17 (2002) 609–618.
[28] E.F. Toro, Riemann Solvers and Numerical Methods for Fluid Dynamics, second ed., Springer, Berlin, 1999.
[29] E.F. Toro, Multi-stage predictor–corrector fluxes for hyperbolic equations, Isaac Newton Institute for Mathematical Sciences, Preprint Series NI03037-NPA, University of Cambridge, UK, 2003.
[30] E.W. Weisstein, CRC Concise Encyclopedia of Mathematics/Eric W. Weisstein, CRC Press, Boca Raton, FL, 1998.